INTERNATIONAL JOURNAL OF CLIMATOLOGY
Int. J. Climatol. (2013)
Published online in Wiley Online Library
(wileyonlinelibrary.com) DOI: 10.1002/joc.3716

RMetS
Royal Meteorological Society

Dominant patterns of US warm season precipitation variability in a fine resolution observational record, with focus on the southwest

Brittany Ciancarelli,[a]* Christopher L. Castro,[a] Connie Woodhouse,[b,c] Francina Dominguez,[a,d] Hsin-I Chang,[a] Carlos Carrillo[a] and Daniel Griffin[b]

[a] *Department of Atmospheric Sciences, University of Arizona, Tucson, AZ, USA*
[b] *Laboratory for Tree Ring Research, University of Arizona, Tucson, AZ, USA*
[c] *School of Geography and Development, University of Arizona, Tucson, AZ, USA*
[d] *Department of Hydrology and Water Resources, University of Arizona, Tucson, AZ, USA*

ABSTRACT: Spatial patterns of interannual variability in US precipitation and their forcing mechanisms are very different between the cool and warm seasons, as determined by the recent observational record. In this work, the dominant continental scale patterns of warm season precipitation variability, in the form of the standardized precipitation index (SPI), are related to their large-scale atmospheric teleconnection forcing patterns. To account for intraseasonal differences in atmospheric teleconnection patterns, the 2-month SPI is considered for the separate periods of early, June–July (JJ), and late, August–September (AS), periods, as well as the 6-month SPI for the cool season (November–April). Rotated empirical orthogonal function analysis and canonical correlation analysis are applied to determine the dominant spatial modes of SPI, their relationship to large-scale teleconnection patterns, and their possible forcing mechanisms, as seen in anomalies of 500-mb geopotential height, sea surface temperature (SST), and outgoing longwave radiation (OLR). Two dominant quasi-stationary Rossby wavetrain teleconnections appear to govern US warm season precipitation variability: (1) a mode that reflects the well-known out-of-phase relationship in summer precipitation between the central United States and southwest, which is related to Pacific SST forcing in early summer and Indian monsoon convection in later summer, and (2) Two phases of the Circumglobal Teleconnection pattern that are more related to precipitation variability in the south central and eastern United States The southwest United States region relating to the variability of the North American Monsoon is considered within the continental scale variability patterns associated with the warm season. This work is a subset of a larger project to determine if tree-ring records from the southwest United States are reliable proxies for extending the warm season climate record. It also provides a benchmark for assessing how US warm season climate patterns may be assessed in regional climate models used for seasonal forecast or climate change projection purposes.

KEY WORDS North American monsoon; US climate variability; teleconnection; North American; warm season; precipitation variability; observational analysis

Received 5 August 2011; Revised 3 April 2013; Accepted 3 April 2013

1. Introduction

Continental scale variability of atmospheric circulation is an important factor in influencing regional climatic patterns over North America. In the realm of this study, the warm season climatology in the broad context of entire United States will be considered to evaluate characteristics of warm season climate variability in the southwest United States. The latter region experiences seasonal maxima in precipitation in both the cool and warm seasons. Cool season precipitation, in the approximate period of November through April, is from the occasional passage of synoptic-scale mid-latitude cyclones, which cause widespread and relatively steady precipitation (Ropelewski and Halpert, 1986). By contrast, during the warm season precipitation is from localized convective storms associated with the North American Monsoon System (NAMS), mainly during July and August (Adams and Comrie, 1997).

It is well known that cool season precipitation in the southwest United States is influenced by large-scale forcing, principally the combination of the El Niño Southern Oscillation (ENSO) and Pacific Decadal Variability (PDV) (Ropelewski and Halpert, 1986, 1987; Redmond and Koch, 1991; Gershunov and Barnett, 1998; McCabe and Dettinger, 1999; Higgins *et al*., 2000; Gutzler *et al*., 2002). These dominant modes of variability, typically viewed via Pacific sea surface temperature (SST) anomalies, change the distribution of convection

* Correspondence to: B. Ciancarelli, Department of Atmospheric Sciences, University of Arizona, Physics and Atmospheric Sciences Building, Room 542, Tucson, AZ 85721, USA.
E-mail: ciancarelli@atmo.arizona.edu

in the tropical Pacific, thereby affecting the large-scale circulation patterns over North America through quasi-stationary Rossby wave teleconnection responses (Horel and Wallace, 1981; Wallace and Gutzler, 1981; Livezey and Mo, 1987; Leathers *et al*., 1991; Biondi *et al*., 2001). During a typical El Niño winter a positive Pacific North America (PNA) pattern is favoured, resulting in a trough over the central North Pacific, a ridge over the northwest United States and western Canada, and a trough over the southwest United States (Wallace and Gutzler, 1981; Blackmon *et al*., 1984; Ropelewski and Halpert, 1986; Trenberth, 1990; Leathers *et al*., 1991; Myoung and Deng, 2009). The subtropical jet over the southern United States is enhanced, and these combined factors cause more frequent and intense mid-latitude cyclones and wetter than average winters in the southwest United States (Hoskins *et al*., 1977; Wallace and Gutzler, 1981; Ropelewski and Halpert, 1986; Mo and Paegle, 2000).

Physical mechanisms influencing the interannual variation of NAMS-associated precipitation has been more challenging to characterize, and is a main focus of our investigation. The positioning and strength of the monsoon ridge modulates the precipitation in southwest and central United States, such that there is an out-of-phase relationship in interannual warm season precipitation variability between these regions (Tang and Rieter, 1984; Okabe, 1995; Higgins *et al*., 1997; Barlow *et al*., 1998; Higgins *et al*., 1998; Castro *et al*., 2001; Castro *et al*., 2007a, 2007b). When the monsoon ridge is strong and positioned anomalously north or northeast of its climatological position, the central United States is relatively dry and hot and the southwest United States monsoon is early and wet. When the monsoon ridge is suppressed to the south with an upper-level trough over the western United States, the central United States is relatively wet on the east side of the trough and the southwest United States monsoon is late and dry (Carleton *et al*., 1990; Harrington *et al*., 1992; Gutzler and Preston, 1997; Mo *et al*., 1997; Higgins *et al*., 1998; Higgins *et al*., 1999; Higgins and Shi, 2000; Castro *et al*., 2001; Castro *et al*., 2007a, 2007b). This out-of-phase relationship in precipitation between the southwest and central United States is the dominant spatiotemporal mode of variability in North American warm season precipitation, varying on a timescale of approximately 9 years (Castro *et al*., 2009).

We offer two possible explanations for the monsoon ridge variability. Antecedent land surface conditions (i.e. snowpack) may affect how fast the land surface is able to heat up during the summer, such that wet (dry) winters would lead to a weakened (stronger) monsoon ridge (Gutzler and Preston, 1997; Gutzler, 2000; Lo and Clark, 2002; Kanamitsu and Mo, 2003; Zhu *et al*., 2005; Castro *et al*., 2009). This idea has been suggested by statistical relationships of antecedent snowpack with monsoon precipitation. The driving hypothesis of our present analyses, as strongly suggested by the prior work in Castro *et al*. (2001, 2007a, 2007b, 2009) is that in addition to land surface forcing, large-scale atmospheric teleconnection patterns related to Pacific SST forcing affect the monsoon ridge position, and thus NAMS rainfall variability over the southwest United States (Mo and Paegle, 2000; Englehart and Douglas, 2006; Mo and Schemm, 2007; Liebmann *et al*., 2008). El Niño-like (La Niña-like) conditions lead to a weak and southward displaced (strong and a northward displaced) monsoon ridge, thereby extending (shortening) the late spring wet period in the central United States and causing a dry and delayed (wet and early) monsoon in the southwest United States (Castro *et al*., 2001, 2007a, 2007b). Moreover, there appears to be distinct atmospheric circulation responses due to ENSO and PDV. Castro *et al*., 2007a, 2007b found that the respective height anomalies statistically related to each are in quadrature, with those over the northern Rockies more related to ENSO and those over the central United States more related to PDV. Thus, as in winter, it is when ENSO and PDV constructively interfere that the dominant mode in warm season precipitation variability is most apparent. Classic example years of where this mode was strongly present and SST-forcing was attributed as a causal factor are 1993 and 1988. The year 1993 was a summer of intense rainfall in the central United States, and it had a dry and delayed monsoon in the southwest United States,1988 was a year of severe drought in the central United States, and a wet and early monsoon (Castro *et al*., 2001). The influence of Pacific SSTs on warm season precipitation variability quickly diminishes after around mid-July. Castro *et al*. (2007a, 2007b) speculate that a possible reason for this is the weakening of the East Asian jet in the western Pacific, which would help diminish the source of Rossby wave forcing in that region (Sardeshmukh and Hoskins, 1988).

Aside from the influence of ENSO and PDV, are there other factors that influence North American warm season precipitation? Another quasi-stationary Rossby wave train pattern in summer is the Circumglobal Teleconnection (CGT), a series of coherent height anomalies across the entire Northern Hemisphere with a zonal wavenumber 5 structure (Ding and Wang, 2005). This teleconnection affects summer precipitation in North America, particularly in the central and southern Great Plains (see Figure 7 from Ding and Wang, 2005). Currently, the driving mechanism of the CGT is not clear. Ding and Wang (2005) propose two possibilities for the generation of the Rossby wavetrain: anomalous Indian Monsoon convection and/or barotropic instability of the mid-latitude westerly jet in the North Atlantic (see their Figure 15). The important point is that the CGT appears to be independent of Pacific SST forcing. Interestingly, the latter possible mechanism for the CGT may also explain some of the statistically significant relationships found between central United States summer precipitation and Atlantic SSTs (Sutton and Hodson, 2005; Feng *et al*., 2011).

The objective of this work is to statistically characterize the dominant modes of US precipitation in the early and late portions of the warm season using high spatial resolution precipitation data, to synthesize

the results of this study with previous studies, and reveal possible mechanisms of teleconnection pattern forcing in a unified analysis framework. The early (JJ) and late (AS) portions of the warm season are considered separately, based on the aforementioned time varying influence of Pacific SST forcing. The specific questions that this paper investigates are: (1) What are the dominant modes of precipitation variability in the warm season?, (2) Do these modes change from the early to late portion of summer?, and (3) What are the possible physical mechanisms that might govern these modes? The specific datasets used in this study are summarized in Section 2. Section 3 describes the analysis methods, including computation of the standard precipitation index (SPI) from the observational precipitation data, rotated empirical orthogonal function (REOF) analysis on SPI, principal component regression, and Canonical Correlation analysis (CCA). Section 4 presents dominant modes of precipitation variability and the relationship to large scale forcing factors. Winter and the early and late summer seasons are analysed separately, with a focus on summertime climate variability. Section 5 considers this observational analysis in the realm of tree-ring data collected from around southwestern United States that is taken into calculations to form a proxy for precipitation. This is part of a larger project that aims to look at NAMS behaviour during drought periods through tree-ring-derived proxy precipitation. Discussion and conclusions are presented in Section 6.

2. Datasets

Aside from the precipitation data, all the following data that are used in our statistical analyses have been obtained on-line from the NOAA Earth Systems Research Laboratory, Physical Science Division (http://www.esrl.noaa.gov).

2.1. Precipitation data

The Parameter-elevation Regressions on Independent Slopes Model (PRISM, 2004) precipitation data is a 0.042 × 0.042 degree resolution monthly dataset over the entire United States from 1895 to present. This product is produced by the PRISM Climate group at Oregon State University and can be retrieved online through the PRISM Climate Group website (http://www.prism.oregonstate.edu). In addition to being a fine resolution dataset, it also includes an algorithm that accounts for changes in topography. For this study, precipitation data from 1895 to 2007 were used and the dataset was mapped to a coarser grid with a resolution of 0.208 × 0.208 degrees due to computer memory limitations. This was done using the meshgrid function in Matlab, which uses information from the original dataset to create a new grid that inputs the data values at the correct location at the specified grid spacing.

2.2. Geopotential height and upper-level wind data

National Center for Environmental Prediction/National Center for Atmospheric Research (NCEP/NCAR) reanalysis global monthly mean 500-mb geopotential height data and mean zonal wind at 200-mb data from the years 1948–2007 are used (Kalnay *et al*., 1996) at a resolution of 2.5 × 2.5 degree grid spacing.

2.3. Sea surface temperature anomaly data

Kaplan SST V2 global monthly sea surface temperature anomaly (SSTA) data (Kaplan *et al*., 1998) consist of a 5.0 × 5.0 degree longitude global grid from 1856 to present. It is produced through statistical methods including empirical orthogonal function analysis (EOF) projection, Optimal Interpolation, Kalman Filtering, Kalman Filter analysis, and Optimal smoothing to fill in the areas of missing data. The SST data obtained by the methods used in Kaplan *et al*. (1998) are based on a mean calculated from the climatological base period 1951–1980. For this study, the monthly anomalies from 1895 to 2007 were used. Although we acknowledge that a higher spatial resolution SST data product could be used, the Kaplan data are of sufficient spatial resolution to capture large-scale patterns of SST variability associated with atmospheric teleconnection responses.

2.4. Outgoing longwave radiation data

NOAA interpolated monthly OLR from 1974 to present is a satellite-derived dataset on a longitude global grid with a resolution of 2.5 × 2.5 degrees (Liebmann and Smith 1996; NOAA Interpolated OLR). The monthly anomalies were computed for this study and the years used were from 1981 to 2007 due to inaccurate data in 1980. Outgoing longwave radiation anomalies (OLRAs) are used as a proxy for tropical convection, with negative (positive) anomalies corresponding to enhanced (suppressed) convection. As the time record of these data are very short, in comparison to the other data, they are used only in the context of physically assessing OLRA associated with teleconnection patterns, not for explicitly assessing the statistical significance of these anomalies.

3. Methods

3.1. Standardized precipitation index

SPI is a normalized value that characterizes anomalous precipitation over a given timescale of interest, typically from 1 to 48 months (McKee *et al*., 1993). The method is especially useful in dry climates of the western United States where precipitation distributions are typically very positively skewed. SPI is a favourable metric for classifying short- and long-term drought because it can be computed at a variety of timescales (Heim, 2002). When viewed as a spatial map, it allows for a more direct comparison of precipitation anomalies at regional and continental scales, and across diverse climate regimes. For this study, different SPI timescales are used for

the cool and warm seasons for the entire period of the PRISM dataset (1896–2007). The cool season is defined using the 6-month SPI from November–April. Although not our primary focus, the cool season is included as a 'check' to verify that the well-known dominant modes of precipitation variability driven by ENSO and PDV forcing are clearly captured by our analysis methods (Ropelewski and Halpert, 1986). For the warm season, 2-month SPI is considered for early (June–July) and late summer (August–September). The warm season is split in such a way to account for the rapidly diminishing influence of Pacific SST forcing on North American teleconnections as the summer progresses (Castro *et al*., 2001, 2007a, 2007b).

3.2. Rotated empirical orthogonal function analysis

To determine the dominant spatial patterns of SPI, REOF analysis is performed on the space-time matrices of SPI data. EOF analysis is computed using a singular value decomposition (SVD) approach (Wilks, 2006). The Varimax rotation method is used, which relaxes the orthogonality constraint of the EOF analysis by maximizing the variance of the squared loadings on a truncated matrix of EOFs (Richman, 1986). Results are shown for rotation of the first five eigenvectors, as the dominant REOF modes were relatively insensitive to a higher number of retained eigenvectors and reflect documented physical modes of climate variability, as will be described in the next section. The principal components of the modes are obtained by projecting the original SPI data onto the REOFs. In all results discussed, modes are displayed consistent with the positive phase of ENSO/PDV or CGT, as documented in previous literature. To compute explained variance of modes, a covariance matrix is first calculated from the original data and divided by the time dimension minus one. The explained variance is then retrieved by multiplying the covariance matrix of the original data with the matrix and transpose matrix of REOFs for the retained modes. The spatial patterns of the modes are shown as the regression of the rotated principal components (RPCs) onto the original data, to have a sense of the magnitude of SPI associated with a given mode. It should be noted that although the periods for the datasets begin at different years for the precipitation and geopotential height (GPH), the consistency of the REOF modes have been confirmed by doing the same REOF analysis on the SPI data for 1948–2007 (figures not shown).

3.3. Principal component regression on large-scale climate forcing indicators

To determine the possible relationship of the dominant REOF SPI modes to large-scale climate forcing, the corresponding RPCs are linearly regressed on the time coincident 500-mb geopotential height anomalies, SSTA and OLRAs. The phasing displayed in the figures is consistent with the phasing used in the Ding and Wang (2005) study for the CGT results (their Figure 7(b)), and also the positive phase for ENSO for the SST regressions. However, each of these respective data span different time periods, as described earlier, reflecting the development of more numerous, sophisticated, and reliable instrumental data collection capabilities through the course of the 20th century.

3.4. Canonical correlation analysis

To verify the results of the RPC regression analyses just described, covariability of SPI datasets with 500-mb (Northern Hemisphere) geopotential height anomalies were assessed using CCA. More importantly, it also is expected that CCA will help reveal the true spatial extent of any large-scale atmospheric teleconnection patterns that may appear in the regressions. The CCA methodology used follows Barnett and Preisendorfer, 1987, as described in on-line notes from Professor Dennis Hartmann at the University of Washington and used previously in Castro *et al*., 2009. SVD is first performed on SPI and 500-mb geopotential height. As in the REOF analyses, the resulting RPCs are truncated to five and normalized by dividing by their respective standard deviations. Again, a higher number of retained RPCs did not substantially affect the results. A correlation matrix of the normalized RPCs is constructed. SVD is performed on the correlation matrix of truncated RPCs in order to obtain the singular vectors corresponding to SPI and 500-mb geopotential height, and the canonical correlations. The singular vectors are projected onto the original truncated RPCs to obtain the canonical correlation vectors. The spatial patterns are finally viewed as either the homogeneous or heterogeneous regression maps with the respective canonical vector.

3.5. Local and field significance

The methods for computing local and field significance of regression and correlation analyses follow those outlined in Livezey and Chen, 1983. Local significance of the principal components from the winter, early summer, and late summer modes correlated with their respective time coincident average geopotential height anomalies, SSTAs, and OLRAs were evaluated using p values less than 0.05. Field significance was then computed on the correlation coefficients for each case using a Monte Carlo technique, where the order of the maps were randomized five hundred times. The geographic area considered for field significance of geopotential height anomalies, consistent with Castro *et al*., 2007a, 2007b, considers only a domain that encompasses the United States and the Atlantic and Pacific basins above 22.5°N to 50°N, and between 140°E and 50°W, as the atmospheric teleconnections signals to US precipitation, though present, are generally not locally significant over Asia and Europe. This was the case for all geopotential height anomaly field significance computations, with the exception the second August/September mode, which considered the entire Northern Hemisphere. Field significance for SSTAs does consider a global domain.

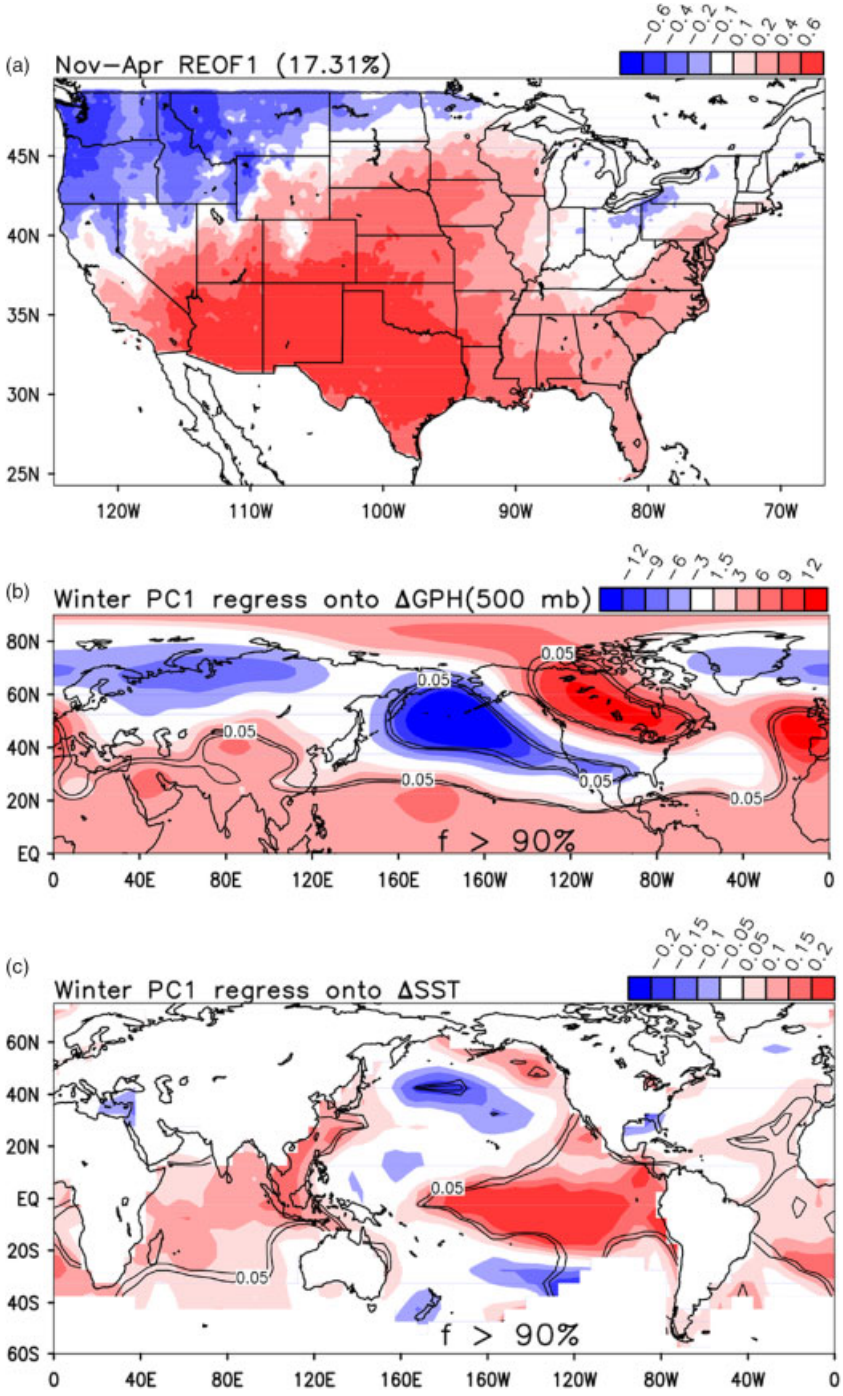

Figure 1. (a) First November–April EOF displayed as a regression of the PC on November–April SPI values. (b) The first November–April PC time series regressed onto average November–April 500-mb geopotential height anomalies (mb), and field significant above 90%. (c) The first November–April PC time series regressed onto average November–April SST anomalies (°C), and field significant above 90%.

4. Dominant modes of warm season precipitation variability in PRISM data

4.1. Cool season-ENSO/PDV signal

The cool season (November–April) is considered to verify the presence of well-known spatial patterns in US precipitation related to ENSO/PDV. It will also be shown that this pattern is an important consideration for the late part of the warm season, in Sections 4.2. and 4.3.. The first dominant mode of cool season precipitation and the associated regression reflects the dominant ENSO/PDV relationship, and explains 17.31% of the variance (Figure 1(a)). There is a strong opposite relationship in precipitation between the Northwest United States and the region encompassing the southwest United States and southern Great plains. Regression of principal component 1 onto 500-mb geopotential height regression reflects the positive phase of the PNA pattern, with a trough over the central North Pacific, and a ridge over the northwest United States and western Canada, and

a trough over the southwest United States (Figure 1(b)) (Wallace and Gutzler, 1981). Regression of this mode onto time coincident SSTAs confirm the well-established relationship of wintertime precipitation variability to ENSO/PDV (Wallace and Gutzler 1981), reflecting locally significant correlation coefficients greater than 0.2 in the eastern tropical Pacific (Figure 1(c)). Although only the dominant mode of cool season SPI is discussed at length, it should be noted that the other well-known modes of winter variability are revealed through the EOF analysis (not shown). The appearance of these well-known wintertime precipitation patterns enhances the confidence in the methods of this study.

4.2. Warm season-ENSO/PDV signal in early summer precipitation

The first REOF and RPC of June–July SPI explains 24.13% of the total variance and confirms the previously noted pattern associated with North American warm season interannual variability (Figure 2(a)). This is the mode associated with the opposite relationship in interannual variability of summer precipitation between the southwest and central United States (Carleton *et al*., 1990; Harrington *et al*., 1992; Gutzler and Preston, 1997; Higgins and Shi, 2000; Castro *et al*., 2001, 2007a, 2007b). The change in sign of the loadings occurs at approximately the Front Range of the Rocky Mountains in Colorado and New Mexico, roughly consistent with the location of the abrupt change of the interannual variability in the diurnal cycle of convection, as noted by Castro *et al*., 2007a, 2007b and displayed in their Figure 3. Virtually the entire southwest region has the same sign of spatial loading, with the strongest negative loadings in Arizona. This monsoon-related precipitation signal extends to approximately 40°N, about the northernmost climatological extent of NAMS rainfall (Adams and Comrie, 1997).

The precipitation pattern represented by the first JJ REOF is related to the evolution and position of the monsoon ridge in North America, as noted in the Introduction and references therein, and this is confirmed with the regression of large-scale climate forcing factors onto rotated RPC 1. The 500-mb geopotential height anomaly regression shows a clear quasi-stationary Rossby wave train originating from the western tropical Pacific, slightly west of the International Date Line (Figure 4(a)), and is field significant above the 90% level. This same analysis was done on 500-mb geopotential height 20th Century Reanalysis V1 dataset from 1908 to 1950 (Compo *et al*. 2006, 2011). This wave train pattern is also revealed and is nearly identical with this dataset, which confirms it is a very robust feature throughout the 20th century (figure not shown). The consistency in the extended reanalysis indicates that this teleconnection arises from a consistent physical forcing mechanism in the climate system that does not substantially vary from the early part of the century to the latter part, as prior statistical analyses of North American warm season precipitation may otherwise suggest (Hu and Feng, 2002). In the positive phase of the mode, the Rossby wave train is related to enhanced convection in the central and eastern Pacific and enhanced convection in the western Pacific, as shown by the OLRA regression in Figure 4(c). The regression on SSTAs (Figure 4(b)) reveals a clear ENSO/PDV signal that is nearly identical to the Combined Pacific Variability Mode (CPVM) in Castro *et al*., 2007a, 2007b and the Pan Pacific mode in Schubert *et al*., 2004, and is field significant above the 90% level. The decadal variability pattern of the RPC time series associated with this mode also confirms the influence of ENSO/PDV. The position of the centre of action over the northern Rockies modulates the monsoon ridge positioning, and is a result of constructive interference of the distinct warm season teleconnection patterns associated with ENSO and PDV (Castro *et al*., 2007a, 2007b). It is also important to note the correlation with SST in the Atlantic off the east coast of Canada, as these reflect the cold phase of the Atlantic Multidecadal Oscillation (AMO). The tropical west North Atlantic warm pool modulates with the AMO, and influences the strength of the North Atlantic Subtropical High (NASH). During the cold phase of the AMO, the strength of the NASH increases, resulting in a stronger Great Plains low-level jet across the southern United States, transporting moisture from the Gulf of Mexico and the Gulf of California into those areas and enhancing the precipitation (Hu and Feng, 2002, 2008; Feng *et al*., 2011).

Covariability of JJ 500-mb geopotential height anomalies and JJ SPI, as determined by CCA, shows basically the same relationship in the first canonical mode, with a canonical correlation of 0.37. There is an opposite relationship between precipitation in the central and southwest United States, with a sharp contrast at the Front Range of the Rockies (Figure 5(a)). The precipitation signal, though, is stronger in the central Great Plains and Midwest, corresponding to a more eastward displacement of the centre of action of the 500-mb height anomaly in Figure 5(b), as compared to that of the RPC 1 regression. This eastward displacement of the 500-mb geopotential height anomaly is more related to PDV, for example as shown in Figure 5 of Castro *et al*., 2007a, 2007b. Regression of the first singular vector of JJ SPI onto SSTA (Figure 5(c)) shows a diminished signature of ENSO when compared to the previous regression of RPC 1 (Figure 4(b)), but there is still a clear SSTA signature in the North Pacific. The negative AMO signal is also present in the CCA analysis.

4.3. Change in warm season ENSO/PDV signal in late summer precipitation

It has been noted that the impact of ENSO/PDV on this large-scale atmospheric teleconnection pattern governing North American summer precipitation diminishes rapidly in the latter part of the summer (Castro *et al*., 2001, 2007a, 2007b). Despite this difference, the first JJ precipitation variability mode still persists as the dominant mode in the AS REOF analysis (Figure 6(a)). This dominant AS

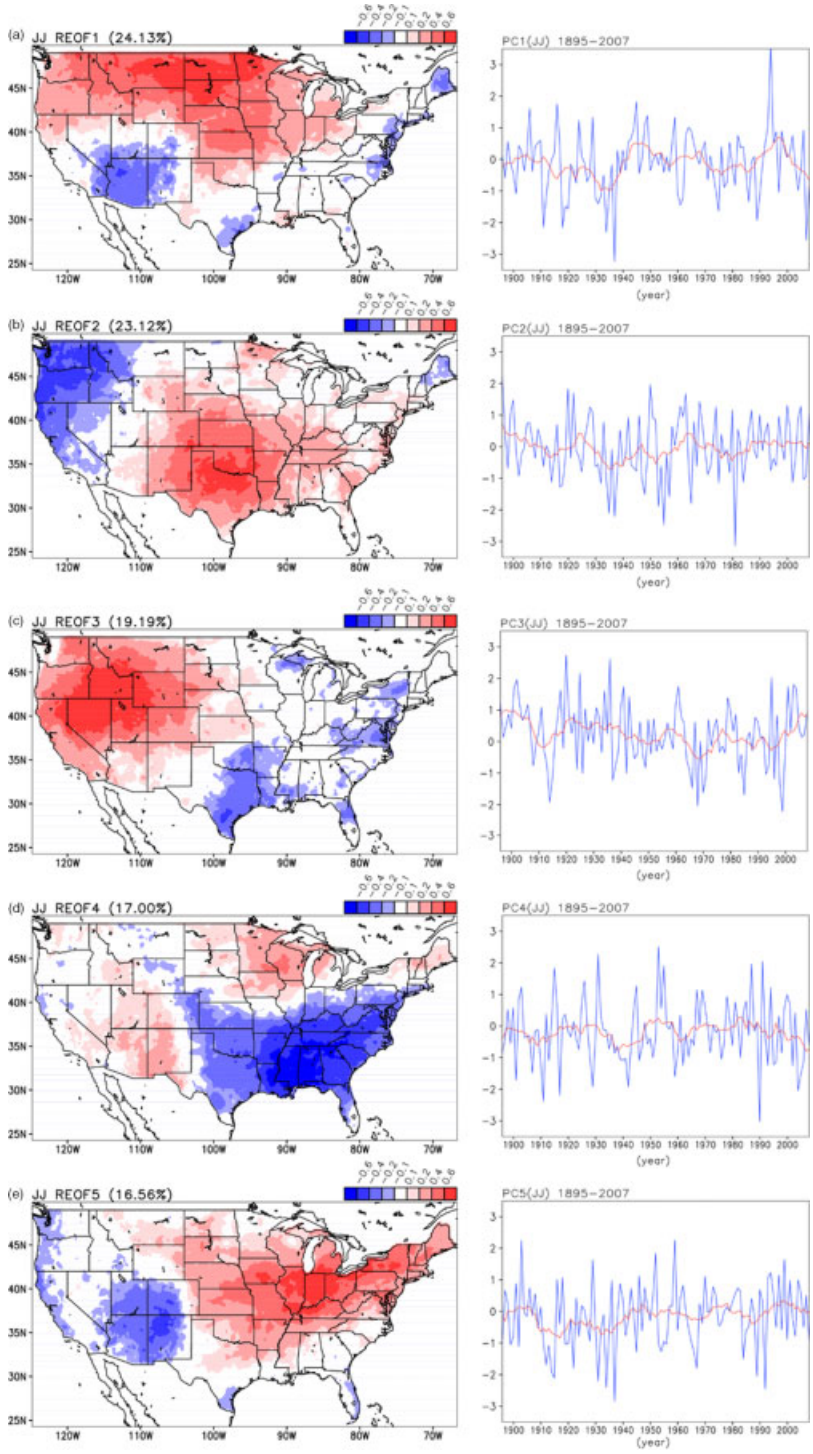

Figure 2. (a) First JJ rotated EOF displayed as a regression of the RPC on JJ SPI values and the first rotated RPC time series with 10-year running average from 1895 to 2007. (b) Same as (a) for second JJ rotated EOF. (c) Same as (a) for third rotated EOF. (d) Same as (a) for fourth JJ rotated EOF. (e) Same as (a) for fifth JJ rotated EOF.

mode explains approximately the same amount of variance as the JJ dominant mode as well. As compared to JJ REOF 1, the spatial loadings diminish somewhat over the southwest and the largest loadings are oriented to the north and west, towards western Arizona, Nevada, and California. There is less of a sharp contrast with precipitation in the central United States. Regression of 500-mb height anomalies on RPC 1 of AS SPI (Figure 7(a)) shows a nearly identical teleconnection pattern to early summer, and has a slightly greater value of field significance at the 89% level. Regression of OLRAs in Figure 7(c) shows suppressed convection in the western Pacific and more importantly, suppressed convection over southeast Asia and the Indian monsoon region. The regression of SSTAs on RPC 1 AS SPI does show the diminished tie to ENSO/PDV (Figure 7(b)), with no ENSO signature

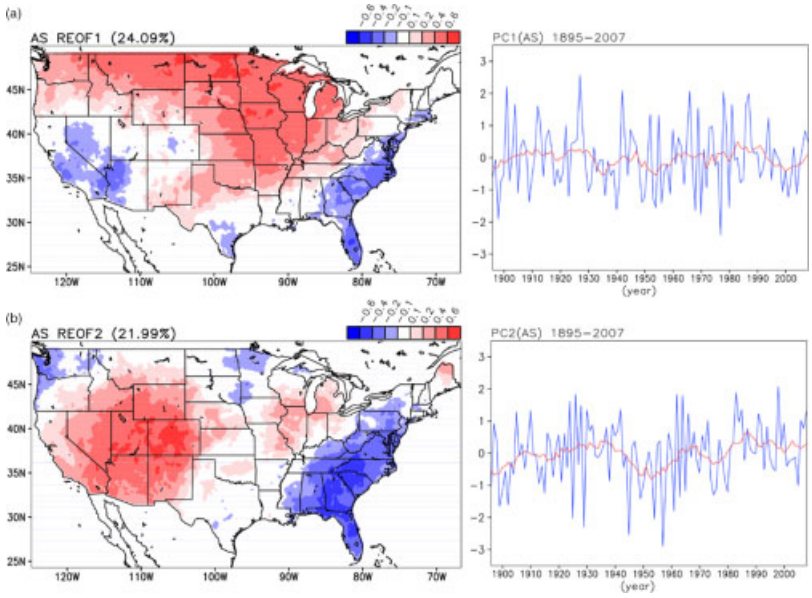

Figure 3. a) First AS rotated EOF displayed as a regression of the RPC on AS SPI values and the first rotated RPC time series with the 10-year running mean from 1895–2007. b) Same as Fig. 3a for second AS rotated EOF.

at all in the eastern Pacific and diminished field significance. We therefore speculate that although exactly the same mid-latitude teleconnection governing the monsoon ridge positioning persists in the latter part of the summer, it becomes increasingly decoupled from equatorial Pacific SST forcing, and likely becomes more dependent on other factors that influence the distribution of tropical convection or otherwise provide a Rossby wave source. That may include the AMO, as its signature is still present in the AS SST correlations (Hu and Feng, 2008). Correlation of the eigenvectors for JJ mode 1 (Figure 2(a)) and AS mode 1 (Figure 6(a)) shows that the precipitation spatial patterns are similar (correlation coefficient 0.7074), which indicates that the pattern is persisting through the late summer. Correlation of the RPC time series for JJ mode 1 and AS mode 1, however, shows that they are virtually statistically independent of each other from the early to the late part of the warm season (correlation coefficient of −0.0484), and therefore supports this hypothesis. The equivalent RPC time series for the latter part of the summer also has less variability on the lower frequency interannual and interdecadal timescales (Figures 2(a) and 6(a)). Variability in Indian monsoon-associated convection may provide more of the source for Rossby wave forcing later in the warm season for this dominant North American warm season teleconnection pattern. The slackening of the upper-level westerly jet in the western Pacific during this time might cause the Rossby wave forcing to shift westward, towards southeast Asia (Sardeshmukh and Hoskins, 1988). An analysis of the 200 mb monthly average u-wind for June, July, and August, shown in Figure 8(a)–(c), respectively reveals this slackening in the jet, as well as the shift in the area of the strongest winds from over the western Pacific to over Tibet. In June, the winds interact with the area of divergence from the strong tropical convection over the western Pacific. By August, the jet slackens and the area of strong wind shifts over Asia, relocating the source region of the Rossby wave train. In addition, the connection of intraseasonal variability of NAMS precipitation to Indian monsoon convection has been shown by Jiang and Lau (2008), with essentially the same teleconnection pattern as shown here.

Another possible reason for the diminishing relationship of late summer precipitation in North America with Pacific SSTAs is revealed by consideration of the second REOF and RRPC of AS SPI in Figure 6(b). This mode explains 22% of the variance, not substantially lower than the first mode. The spatial pattern of this mode, though, is more indicative of the classic ENSO/PDV cool season signature as discussed before in Section 4a and in Figure 1(a), with positive precipitation anomalies in the southwest United States and negative precipitation anomalies in the Pacific northwest and southeast United States. Correlation of the first and second AS RPCs shows that these are two distinct patterns influenced by two different physical mechanisms (correlation coefficient −0.08). Regressions of RPC 2 of AS SPI with OLRA (Figure 9(c)) and SSTA (Figure 9(b)) confirm that this more cool-season type pattern is related to ENSO/PDV forcing, as they are quite similar to what is observed for the cool season period of November–April in the first REOF mode (Figure 1(c)), and are field significant above the 90% level. In the 500-mb geopotential height regression, the PNA pattern is not as well-defined (Figure 9(a)). The second AS mode of SPI destructively interferes with the first mode in the southwest because the spatial loadings are of opposite sign from the first mode. So the late summer may also simply be a period of transition in ENSO/PDV teleconnective relationships that affect warm and cool season precipitation in the western United States. Thus, there would not be a strong tie of AS NAM

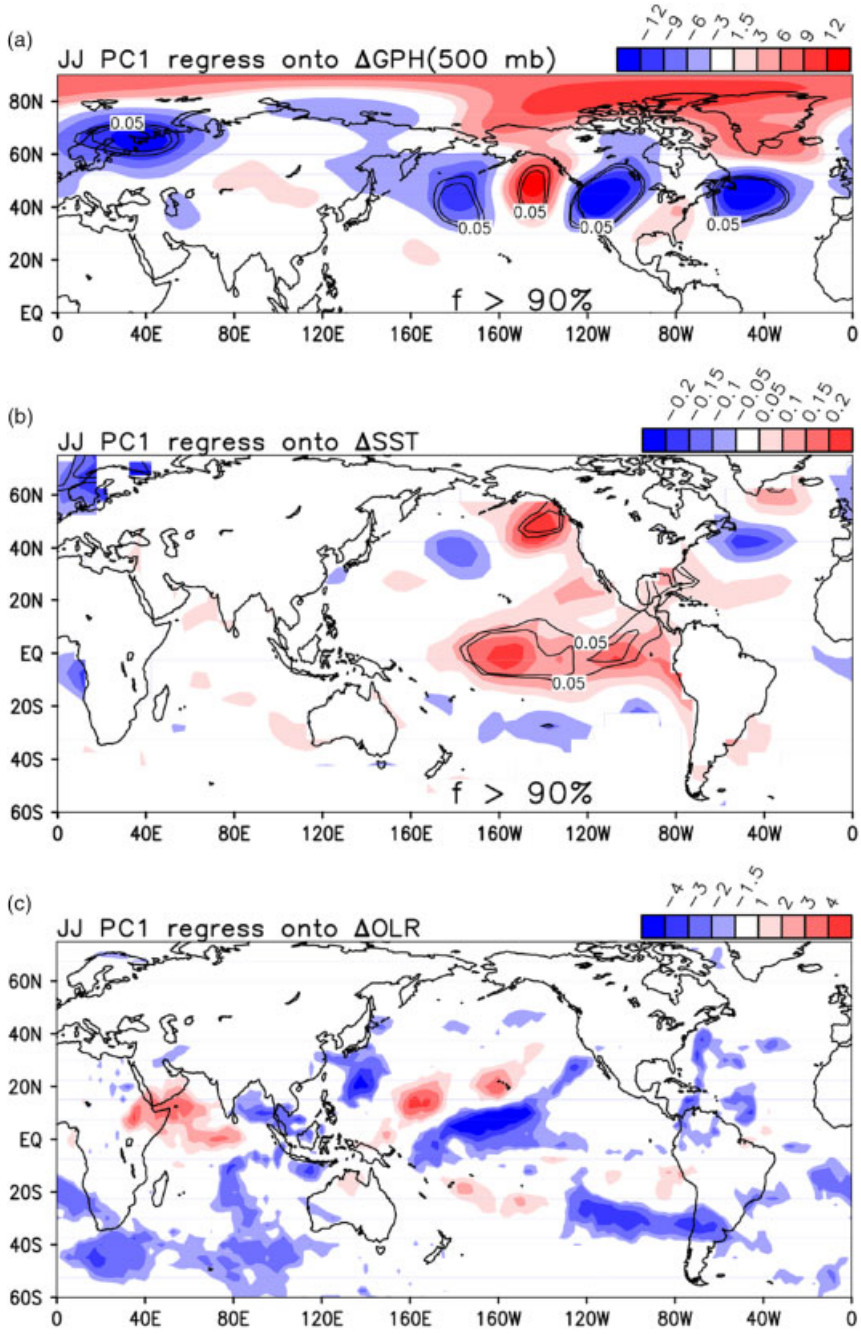

Figure 4. (a) The first JJ rotated RPC time series regressed onto average JJ 500-mb geopotential height anomalies (mb), and field significant slightly above 85%. (b) The first JJ rotated RPC time series regressed onto time average JJ SST anomalies (°C), and field significant above 90%. (c) The first JJ rotated RPC time series regressed onto average JJ OLRAs (Wm^{-2}).

precipitation to remote Pacific SST forcing as these signals would cancel each other out when considering North American relationships with Pacific SST indices or dominant spatial modes of SSTA variability, as done earlier in Castro *et al*., 2001, 2007a, 2007b, respectively.

CCA analysis of AS SPI (figures not shown) with time coincident geopotential height anomalies confirms the diminished influence of ENSO/PDV in the later part of the summer. The second singular vector displays a precipitation variability pattern similar to that of the first AS mode, with both showing the highest spatial loadings in the southwest United States. The geopotential height anomaly pattern reflected through this singular vector is identical to the late summer dominant mode, as well as to the dominant mode of early summer. Regression onto time-coincident SSTAs reveals no correlation with Pacific SSTAs, which gives additional evidence supporting the lack of influence of ENSO/PDV in late summer. The CCA counterpart to AS REOF 2 is revealed in the fifth singular vector and is not shown in the figures.

4.4. Intermountain West precipitation mode

The third dominant mode of JJ is related to early warm season precipitation in the Intermountain West, with

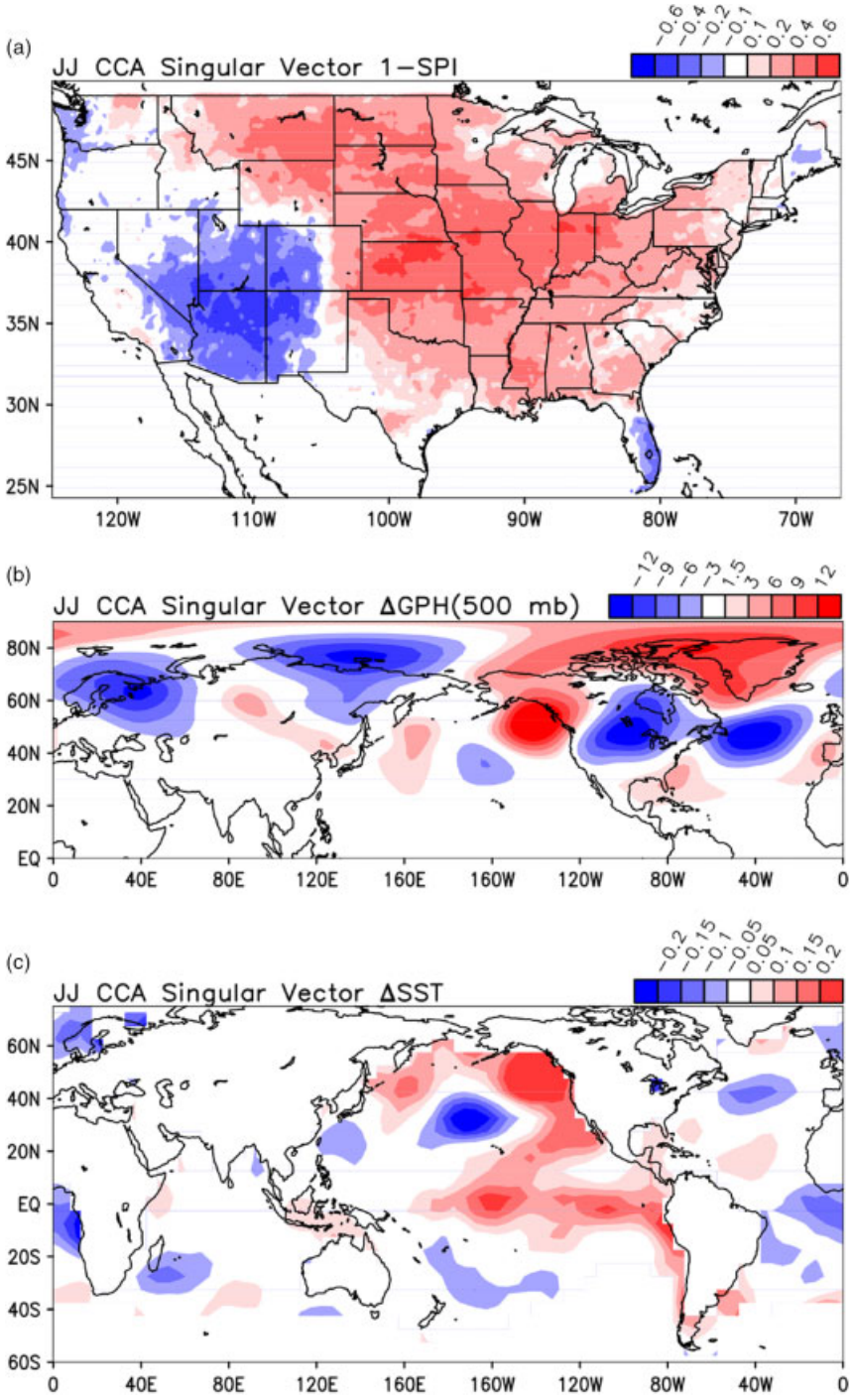

Figure 5. (a) Homogeneous map of first SPI singular vector from CCA on time coincident JJ SPI and average JJ 500-mb geopotential height anomalies (SPI). (b) Heterogeneous map of JJ 500-mb geopotential height anomalies regressed onto first singular vector of JJ SPI (mb). (c) Heterogeneous map of JJ SSTAs regressed onto first singular vector of JJ SPI (°C).

the strongest loadings on the northern periphery of the North American Monsoon in the Great Basin region (Figure 2(c)), and explains 19% of the variance. The associated teleconnection pattern, field significant over the 90% level, extends over the Northern Hemisphere and shows a strong anomalous low (high) over the West and additional height anomalies over the Pacific Ocean in the positive (negative) phase of the mode (Figure 10(a)). This is somewhat consistent with the early summer teleconnection pattern and monsoon ridge positioning associated with just ENSO, as shown in Castro *et al*. (2007a, 2007b, their Figure 5) for the time period late June to early July. The regression of this RPC onto SSTAs, however, reveals only a 35% field significance, with only a small area that is locally significant in the Niño 1 and 2 regions (Figure 10(b)). OLRA appears to be strongly ENSO influenced, with suppressed and enhanced convection over the western and eastern Pacific,

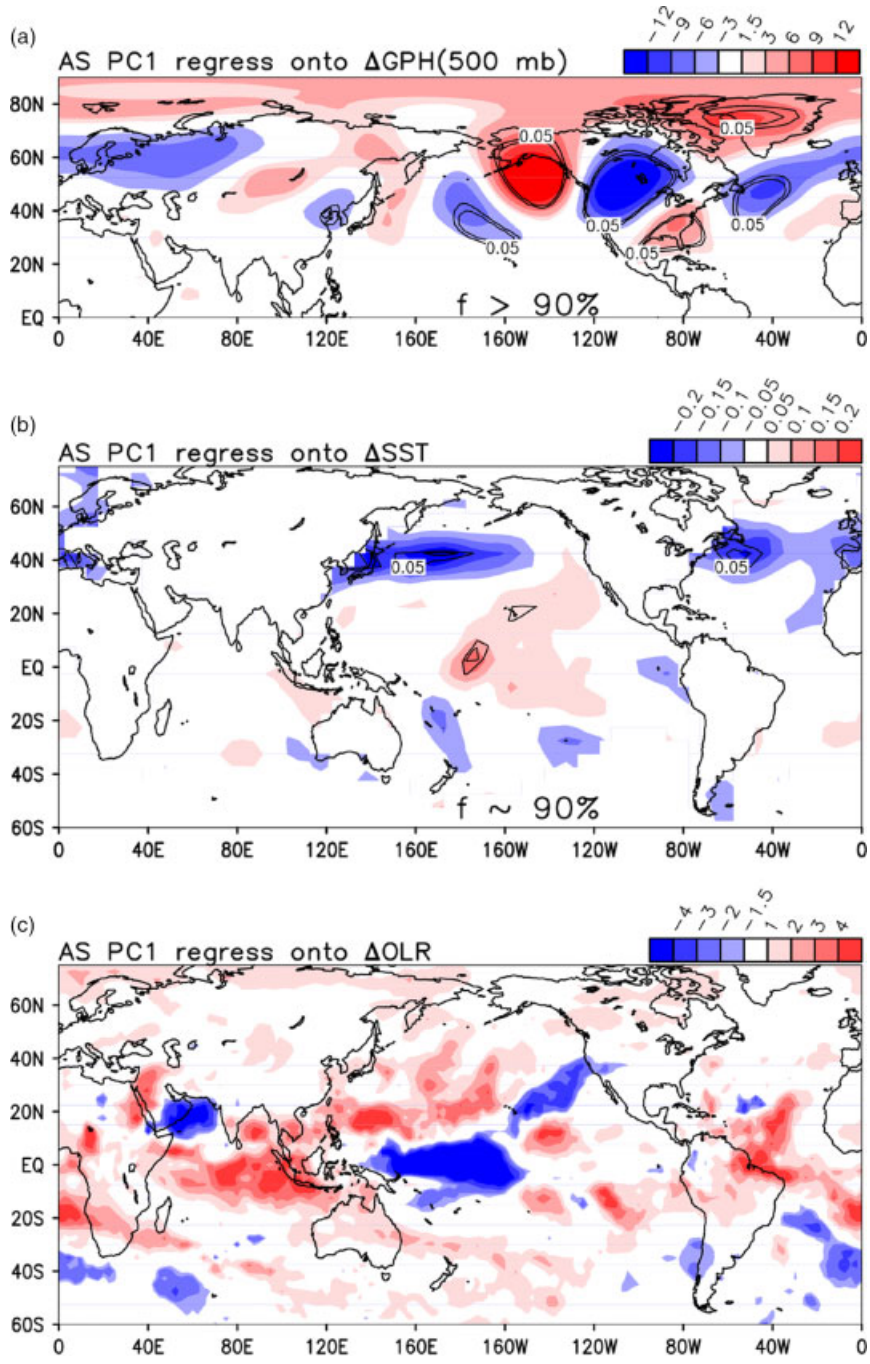

Figure 6. (a) The first AS rotated RPC time series regressed onto average AS 500-mb geopotential height anomalies (mb), and is field significant at about 89%. (b) The first AS rotated RPC time series regressed onto time average AS SST anomalies (deg. C), and is field significant at about 90%. (c) The first AS rotated RPC time series regressed onto average AS OLRAs (Wm^{-2}).

respectively, for the positive phase of the mode (Figure 10(c)). This mode is consistent with the CCA JJ fifth singular vector (figures not shown).

This result is interesting, in that it does not seem to be primarily influenced by SSTAs, as revealed by the low field significance in the SSTA regression. This mode requires further study and investigation to determine the physical mechanism behind it. Although there is not a long-term trend in this third JJ mode considering the respective RPC time series of the entire 20th century (Figure 2(c)), there is a slightly negative trend since the 1960s, possibly related to increasing early summer dryness in the intermountain west. Is the recent trend in this mode and intensification of the geopotential height anomalies in the western United States reflective of a synergistic interaction between Pacific-SST variability and anthropogenic climate change that is intensifying early warm season drying? There is an absence in correlation between the SPI and the natural SST forcing, which suggests that another mechanism is the primary influencing factor, although it is not clear from this study that climate change is that factor. It has been posed as a

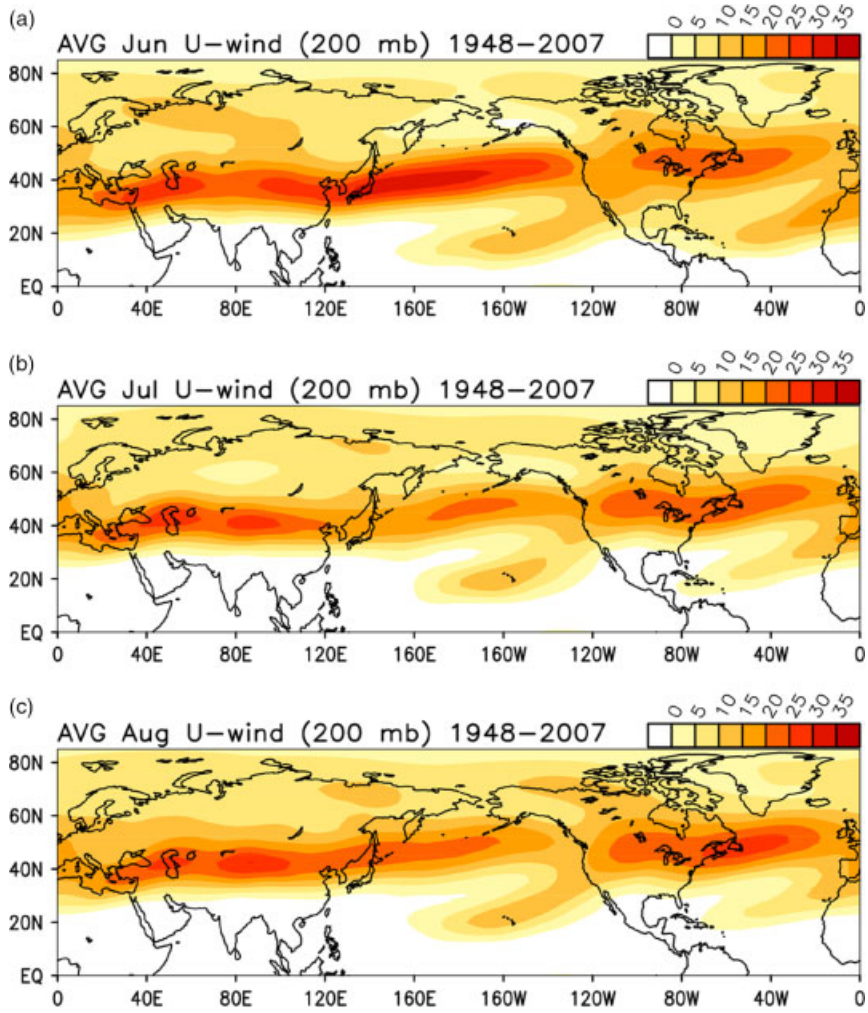

Figure 7. (a) Average June 200 mb u-wind (ms^{-1}). (b) Average July 200 mb u-wind (ms^{-1}). (c) Average August 200 mb u-wind (ms^{-1}).

plausible hypothesis by previous studies, however (Weiss *et al*., 2009).

4.5. Circumglobal teleconnection signal in warm season precipitation

In contrast to Ding and Wang 2005, our analysis suggests that the June and July patterns of the CGT identified in that study are in fact two statistically distinct modes of this teleconnection pattern, which can occur in either month. The second JJ SPI mode reflects a precipitation pattern with an opposite relationship between the Northwest and Southern Great Plain regions (Figure 2(b)) and explains 23.1% of the variance. JJ geopotential height anomalies regressed onto JJ RPC 2 (Figure 11(a)) reflects a very similar pressure anomaly pattern to Ding and Wang's July expression of the CGT (Ding and Wang, 2005, Figure 7(b); Ding *et al*., 2011, Figure 11). Locally significant geopotential height anomalies do not extend completely around the Northern Hemisphere, but this is expected *a priori* considering precipitation data is restricted to just the United States.

The pattern represented in the second JJ SPI mode is also present in fourth JJ SPI geopotential height anomaly CCA results. Regression of this mode of variability onto time-coincident SSTAs does not show any strong statistical relationship and coherent pattern of global SSTA (Figure 11(b)), suggesting that ENSO/PDV variability is not the primary physical cause for it, very much unlike the dominant JJ mode discussed in the previous section. The relationship to JJ OLRAs, however, shows that there is correlation with enhanced convection in the Indian subcontinent (Figure 11(c)). Thus, it is plausible that the CGT expression connected to this mode of precipitation variability could be influenced by Indian Summer Monsoon convection, and this is entirely consistent with one of the hypothesized physical mechanisms posed by Ding and Wang (2005).

The June expression of Ding and Wang's CGT pressure anomaly composites (Ding and Wang, 2005, Figure 7(a); Ding *et al*., 2011, Figure 11) emerges as the fifth mode of JJ SPI variability (Figure 2(d)) and explains 16.6% of the variance. The precipitation anomaly pattern shows the highest loadings in the Northeast and Great Lakes portion of the United States, which is similar to the precipitation anomaly pattern shown in their figure. In the regression of the JJ geopotential height anomalies onto the fifth RPC

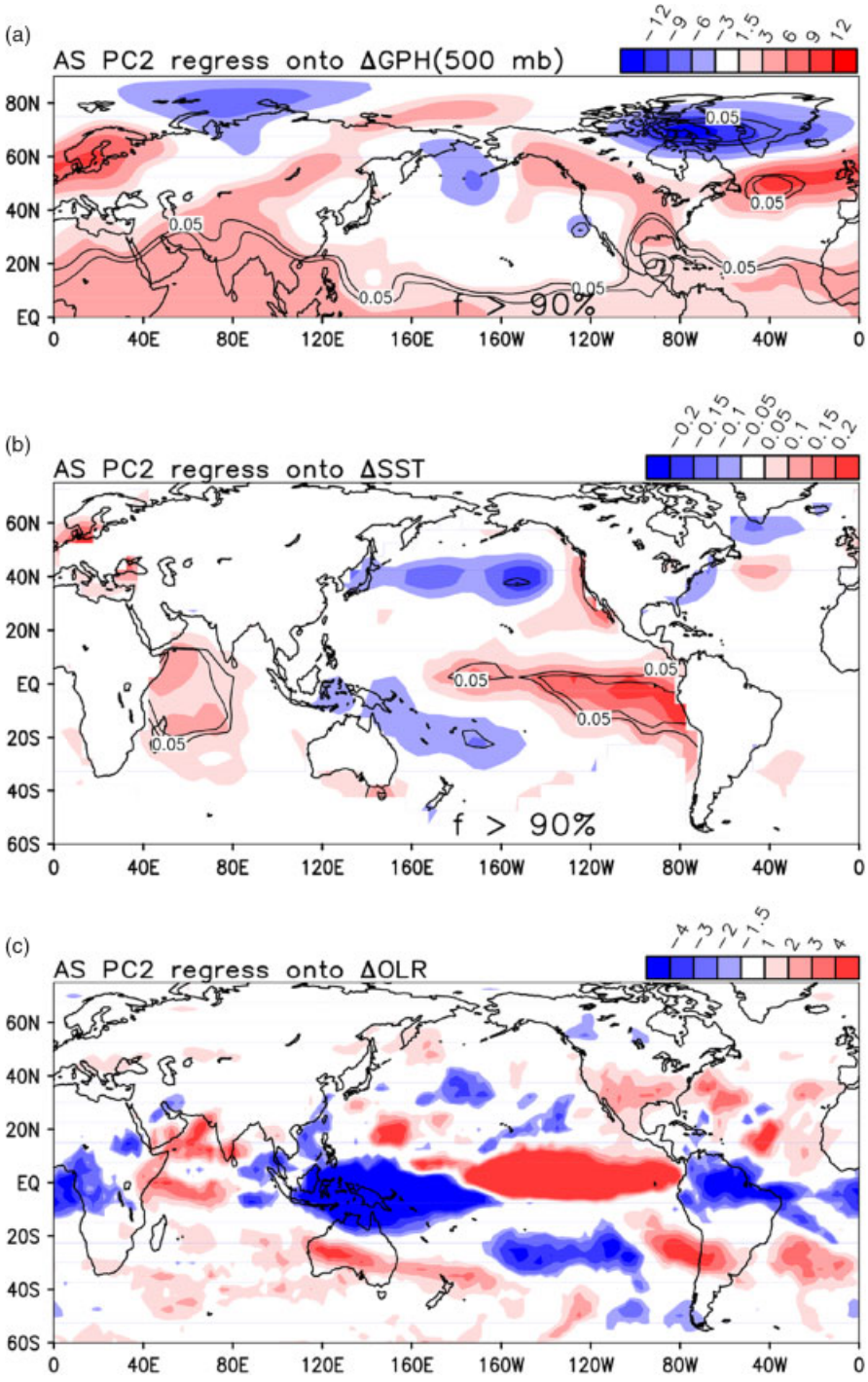

Figure 8. As in Fig. 6 (a) [field significant above 90%], (b) [field significant above 90%], and (c) for AS RPC 2.

the anomalies displayed are of opposite sign and slightly shifted, however, the pattern is similar and field significant is at the 82% level (Figure 12(a)). As before, the most locally significant geopotential height anomalies are closest to North America. In the geopotential height SPI CCA analysis, this pattern appears as the third coupled mode. Regressing time coincident SSTAs onto this REOF mode again shows little relationship to tropical Pacific SSTAs (Figure 12(b)), though there is a relationship to the distribution of convection in the western Pacific and southeast Asia (Figure 12(c)) that is somewhat similar to the possible forcing areas described in Ding and Wang, 2005 and Jiang and Lau, 2008.

The opposite relationship in precipitation between the Northwest and Southern Great Plains for the later part of the summer (AS) appears in the fifth mode of the REOF analysis. It reveals even stronger loadings in the latter region and explains 17% of the variance. As the characteristics of this AS mode are nearly identical to early summer JJ REOF 2, it is not shown. A persistent phase of this CGT mode during the summer would affect precipitation in the Southern Great Plains, particularly

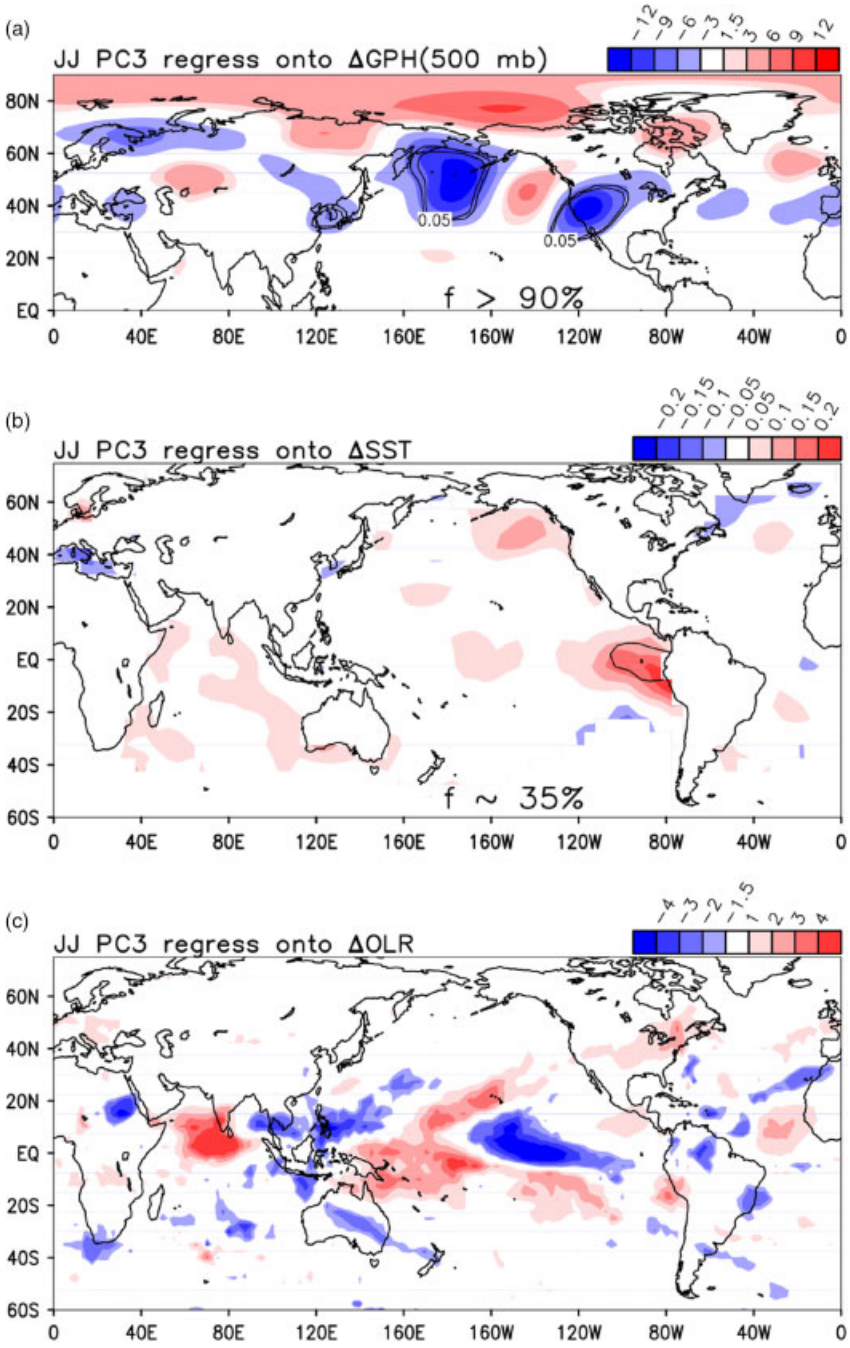

Figure 9. As in Fig. 4 (a) [field significant at about 69%], (b) [field significant at about 35%], and (c) for JJ RPC 3.

Texas. The recent extreme summer drought in Texas during summer 2009 is a very good example of where this mode was strongly present throughout the warm season over North America (Tardy, 2010). Again, there is no correlation between global SSTAs for this AS mode. The relationship with OLRAs reveals the continued tie to Indian Summer Monsoon variability and tropical convection in the western Pacific that persists from the early summer. The corresponding CCA analyses shows this as the fourth coupled mode. It is worth noting that these two expressions of the CGT also have a pattern of correlation that reflects a possible connection to the AMO, and this is important given that the CGT precipitation modes are associated with warm season precipitation more in the central and eastern United States.

5. Connecting PRISM precipitation data analysis to paleoclimate

5.1. Southwest United States latewood tree-ring data as proxy for warm season precipitation

The southwest United States first systematic network of monsoon-sensitive tree-ring chronologies is currently being developed through the University of Arizona at the Laboratory of Tree Ring Research (see Griffin

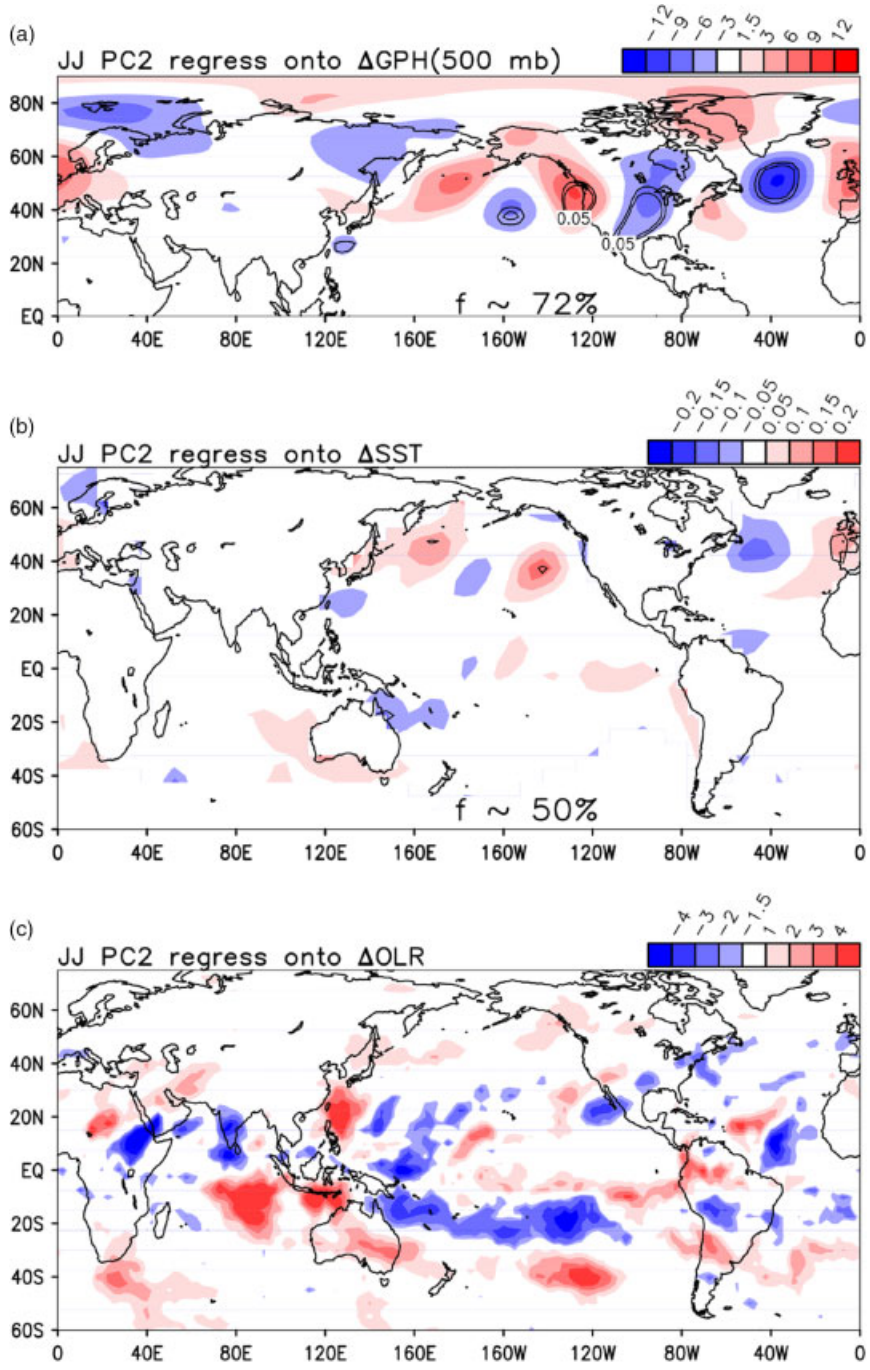

Figure 10. As in Fig. 4 (a) [field significant at about 55%], (b) [field significant at about 50%], and (c) for JJ RPC 2.

et al., 2011; Leavitt *et al*., 2011). Monsoon-sensitive chronologies are derived from the dark-coloured summer growth component of annual tree-rings in southwestern conifers, and have been previously demonstrated to be sensitive to monsoon precipitation (Meko and Baisan, 2001; Therrell *et al*., 2002; Stahle *et al*., 2009). The new network of chronologies will be used to develop regional reconstructions of monsoon precipitation that extend to the past 300–500 years, with results that will be used to evaluate drought history through analyses such as time slice principal component analysis and observing dominant rainfall variability modes back through time. The dominant modes of precipitation variability retrieved from this study will later serve as a rough observational baseline for comparison with dominant modes computed from tree-ring-derived precipitation for the southwest United States.

The primary purpose of this network is to develop a set of regional reconstructions of warm season precipitation for the southwest using the latewood ring widths of *Pinus ponderosa* (ponderosa pine) and *Pseudotsuga menzeseii* (Douglas-fir) trees, from a spatially dense network of monsoon-sensitive tree-ring chronologies around the area. Growth rings are composed of an earlywood and

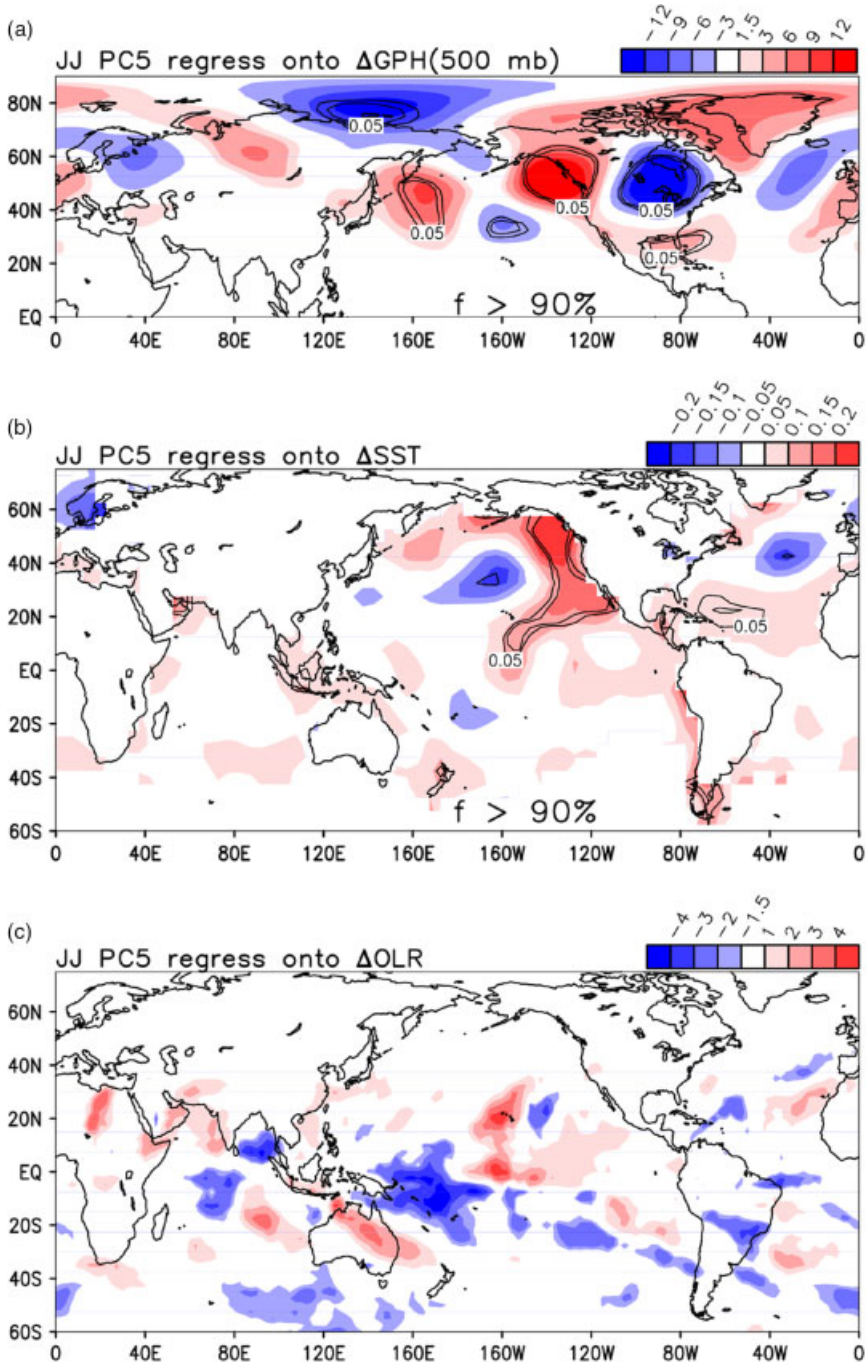

Figure 11. As in Fig. 4 (a) [field significant at about 82%], (b) [field significant at above 90%], and (c) for JJ RPC 5.

latewood portion, with the latewood corresponding to summertime climate (Meko and Baisan, 2001). From this latewood portion, a latewood adjusted index (LAI) is computed and used as a proxy for precipitation. A similar REOF analysis approach as performed in this study is used to define regional patterns of the NAM using the set of adjusted latewood chronologies. Exact replication of the observational results presented in Section 4 is not expected due to the sensitivity of EOF analysis to spatial domain, which is different between the observational analysis and the tree-ring analysis. Also, since the tree-ring collection sites are scattered throughout the NAM region, the trees are likely to have variable responses to the climate based on the proximity to NAM influence and the physiographic setting (Fritts, 1966). If the trees are accurately representing the general spatial variability of NAM season precipitation documented in the instrumental data, then this gives much greater confidence that the extended record of NAMS rainfall will document regional patterns of the NAM going back hundreds of years.

Currently, the NAM precipitation reconstruction project involves a network of tree-ring chronologies from 50 sites in different mountain chains around the southwest United States (36 of these collections were available

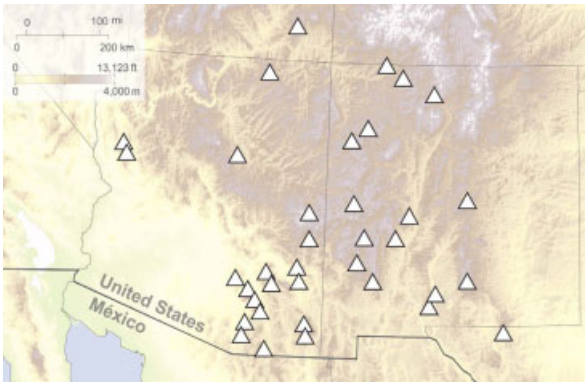

Figure 12. This map illustrates the distribution of the 36 tree-ring collection sites (red triangles) which have been updated to 2008 for inclusion in our analysis.

at the time of this study). Of these sites, more than half were collected from the core NAM region in southeastern Arizona and southwestern New Mexico. Most of the other sites are on the fringe of the NAM area, including NV, UT, CO, and TX. The width of the two parts of the annual growth ring, the earlywood and latewood, are measured separately to generate the LAI chronologies that can reflect warm season moisture variability. These latewood chronologies are currently under development through the Laboratory of Tree Ring Research at the University of Arizona. Griffin *et al*. (2011) describe the development strategies for these latewood chronologies, as well as the bias corrections, and showcases NAM sensitivity results using four of them from the core NAM region.

5.2. Rotated EOF analysis of latewood adjusted index

A preliminary analysis to observe the spatial variability of NAM precipitation, as indicated through the latewood portion of the tree-rings, has been completed using 36 sites around the southwest (Figure 3). LAI serves as a proxy for precipitation, with the RPCs representing dominant modes of tree growth, and these modes are correlated to regional patterns of SPI (Meko and Baisan, 2001). These dominant modes from the latewood adjusted time series are retrieved using rotated EOF analysis from 1895 to 2007. Correlation of the first five RPCs with July–August (JA) PRISM SPI reveals the dominant modes of tree growth, which are correlated to patterns of precipitation variability associated with the NAM in different areas of the southwest. The first REOF shows high correlations in the core NAM region with the maximum values located in southern Arizona (Figure 13(a)), and explains 17% of the variance. It should be noted that JA SPI was used in this portion of the study, despite the mixed early/late summer seasonal signal in the climate data. The statistical relationship between tree growth and monsoon precipitation is stronger with July and August than with June in large part because we are using monthly data, and in this region, June is typically dry until quite late in the month. Since the onset of the Monsoon is not until later in June, the response in tree growth to that onset is not observed in the tree-ring data until July. In the eastern portion of the tree-ring study area, June is more important because the onset of the NAM is earlier in the month of June.

Are these tree-growth RPCs reflecting large-scale variability in geopotential height anomalies and SSTAs? Correlation of LAI RPC 1 with time coincident JA SSTAs reveal a clear ENSO/PDV signature in the northern Pacific, and tropical eastern to central Pacific (Figure 13(c)). An ENSO/PDV signature is also apparent to varying degrees in the second, fourth, and fifth modes (not shown). The correlation between this mode and JA geopotential height anomalies show expected teleconnection response pattern extending from the tropical Pacific over North America, with an origin point in the western tropical Pacific (Figure 13(b)). This circulation pattern, however, is not quite as clear as the ENSO/PDV dominant JJ SPI mode highlighted in section 4b of this study. A link between summer climate variability in the southwest United States and ENSO/PDV has been found in previous studies (Stahle *et al*., 2009). Stahle *et al*. (2009) investigated NAMS precipitation using a 2139-year-old tree-ring-based precipitation reconstruction from north central New Mexico, and found an antiphase relationship between winter and summer precipitation characteristic of ENSO/PDV variability. This preliminary analysis strongly supports the hypothesis that latewood tree-ring data are a reliable paleoclimate proxy to capture monsoon precipitation interannual variability, and extends the earlier work of Stahle *et al*. (2009) to now consider the associated spatial patterns. Our next phase of work will use these data to investigate monsoon precipitation and its relationship to Pacific SST variability using reconstructions of climate from the latewood portion of tree-rings, with an emphasis on NAMS behaviour during drought periods documented in other regional hydroclimatic reconstructions (Woodhouse *et al*., 2006; Meko *et al*., 2007).

6. Discussion and conclusions

This work provides a unified framework for the statistical analysis of early and late warm season precipitation variability over the United States, using the high-resolution PRISM product. Our results are consistent with prior work that has investigated the influence of large-scale atmospheric teleconnections at this time of year accounting for the distinction between the early and late warm season. PRISM also better accounts for the influence of topography than other more coarsely resolved precipitation data that has hither to for been used, resulting in a more accurate depiction of spatial patterns of precipitation variability. Observing the early summer (June/July) and late summer (August/September) separately shows that there are different large-scale teleconnective influences that control over precipitation variability in North America that change in time. When considering the early summer, the relationship of SPI spatial variability to

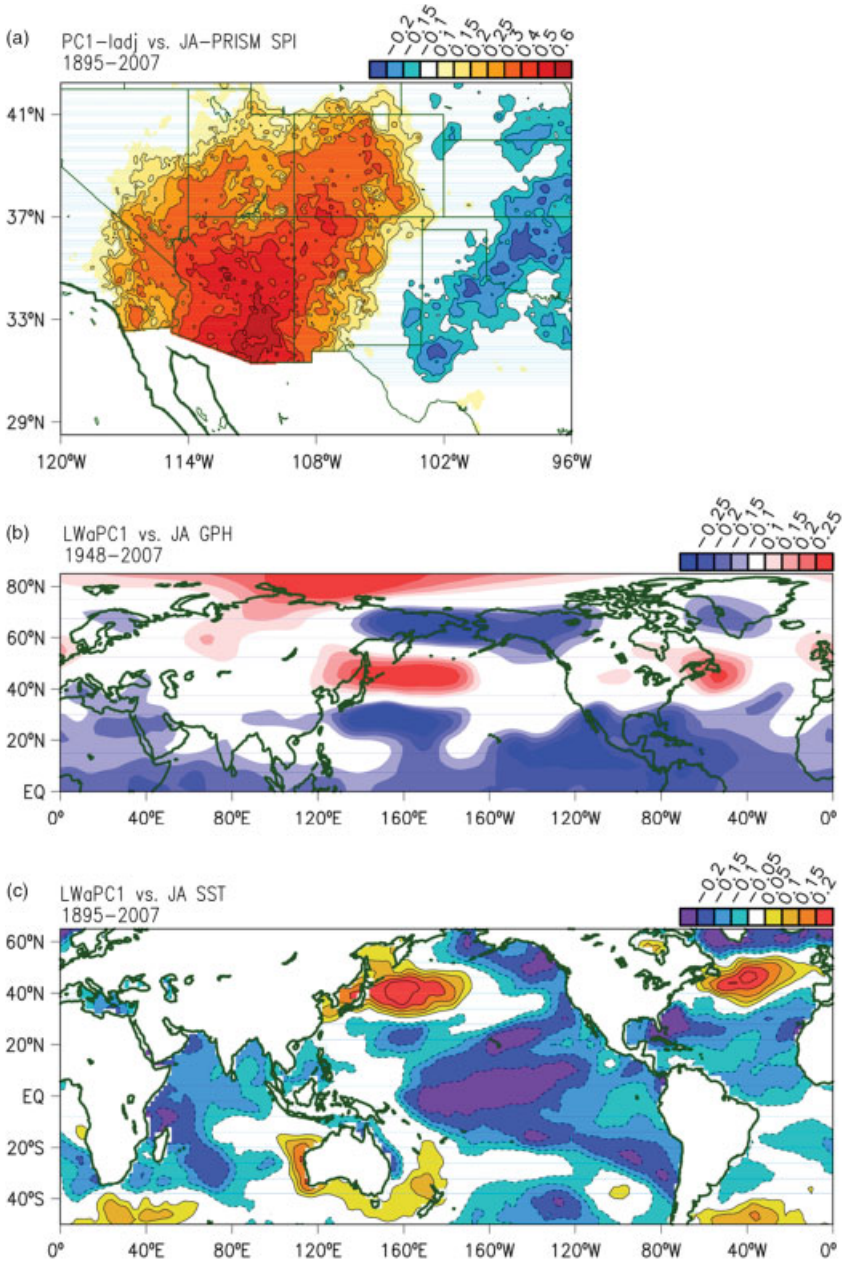

Figure 13. (a) The first LAI rotated RPC time series regressed onto average JA PRISM SPI. (b) The first LAI rotated RPC time series correlated with average JA 500-mb geopotential height anomalies. (c) The first LAI rotated RPC time series correlated with time average JA SST anomalies.

dominant modes of SST variability (ENSO/PDV, AMO) is reflected in the dominant modes, which in turn influences the positioning and strength of the NAM ridge (Figure 14(a) and Table I) (Castro *et al*., 2001, 2007a, 2007b). Another important observation to note is that the strongest loadings of variability in the dominant JJ modes are in the vicinity of the NAM region. The extent of NAM precipitation is also accurately depicted through this mode, which is in part due to the inclusion of elevation effects in the PRISM data. This highlights the importance of topography in NAM precipitation spatially over the United States. When considering tree-ring data, these tree coring sites are located in the higher elevations and therefore are physiogeographically well positioned to capture this variability.

The relationship of western and central United States summer precipitation to Pacific SSTAs has been noted in previous literature to wane in late summer, and our analysis confirms this (Table I). The geopotential height anomaly patterns between early and late summer are nearly identical for the dominant precipitation mode, but as the polar jet stream in the western Pacific slackens in late summer, the origin of the Rossby wave forcing shifts upstream further west to southeast Asia and India (Figure 14(b)). Thus the mode becomes increasingly decoupled from Pacific SST forcing from late July onward and more dependent on the variability in Indian and Southeast Asian monsoon convection (Sardeshmukh and Hoskins, 1988, Jiang and Lau, 2008). In addition, when considering the second late summer precipitation

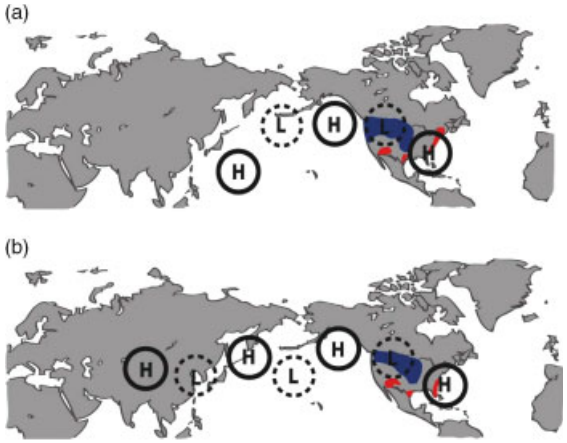

Figure 14. (a) Idealized atmospheric teleconnection pattern associated with JJ REOF 1 (ENSO/PDV forcing dominant). (b) Idealized atmospheric teleconnection pattern associated with AS REOF1 (likely dependent on Asian monsoon convection). Wet/dry areas over the United States indicated by blue/red.

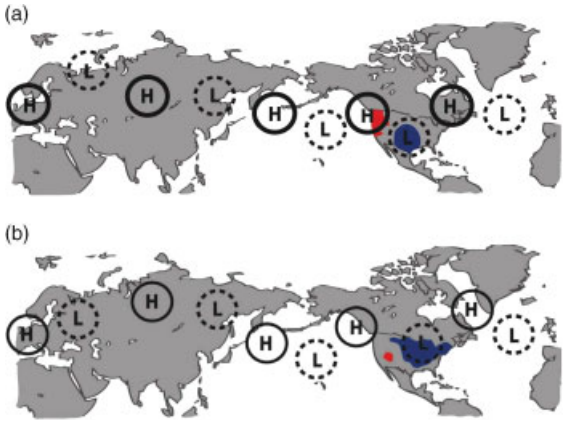

Figure 15. (a) Cartoon illustrating the CGT atmospheric teleconnection pattern associated with JJ REOF 2 (likely associated with the CGT). (b) Cartoon illustrating the CGT atmospheric teleconnection pattern associated with JJ REOF 5 (likely associated with the CGT). Wet/dry areas over the United States indicated by blue/red.

Table I. Winter, early, and late summer EOFs, explained variance, and forcing mechanisms.

EOF ranking	Explained variance (%)	Forcing mechanism
Winter EOF 1	17.31	ENSO/PDV
JJ REOF 1	24.13	ENSO/PDV, AMO
JJ REOF 2	23.12	CGT
JJ REOF 3	19.19	Climate change?
JJ REOF 4	17.00	ENSO/PDV, AMO
JJ REOF 5	16.56	CGT
AS REOF 1	24.09	Indian/SE Asian monsoon convective variability/North Atlantic Westerly Jet Barotropic instability
AS REOF 2	21.99	ENSO/PDV
AS REOF 5	16.99	CGT

mode it reflects more ENSO/PDV relationships associated with cool season precipitation, in opposition to the dominant mode. These combined effects result in a diminished influence of Pacific SSTAs on late summer US precipitation variability.

In both the early and late warm season, precipitation variability is also related to the CGT, which is thought to be driven by Indian Summer Monsoon convection or barotropic instability in the North Atlantic sector of the mid-latitude westerly jet (Ding and Wang, 2005). This study confirms the existence of the CGT. But the two expressions of the CGT pattern previously described by Ding and Wang (2005) to be respectively specific to June or July, can, in fact, occur in either month. While Ding and Wang (2005) and Ding *et al*. (2011) took a top-down approach, characterizing the large scale teleconnection patterns first before relating them to the localized precipitation patterns, this study has focused on examining the localized precipitation first, and then connecting those patterns to the large scale influences. One expression of the CGT is associated with an opposite relationship in SPI between the Southern Great Plains and the Northwest (Figure 15(a)). The other expression is associated with the highest variability in the Northeast and Great Lakes region of the United States (Figure 15(b)). It is also important to note that the CGT pattern is associated with precipitation variability in the Southern Great Plains and is a consistent pattern throughout the warm season. If this pattern is present then anomalous wet or dry conditions can potentially exist throughout the summer season in this region, creating extreme wet or dry conditions. Figure 15(a) and (b) is consistent with the findings of Ding *et al*. (2011), Figure 12.

As mentioned, some studies have hypothesized that antecedent land surface conditions, like snowpack, and land–sea thermal contrast are important to warm season precipitation variability over the United States (Gutzler and Preston, 1997; Gutzler, 2000; Lo and Clark, 2002; Kanamitsu and Mo, 2003; Zhu *et al*., 2005; Castro *et al*., 2009). Our statistical analysis, strongly suggests that the large-scale teleconnection responses shown in this study are all associated with remote forcing, and are the first order factors on United States warm season precipitation climate variability (Castro *et al*., 2007b; Ding and Wang, 2005; Jiang and Lau, 2008). The remote forcing mechanisms influence the development of quasi-stationary Rossby wave train patterns, and therefore the distribution of large-scale circulation anomalies over North America. More relevant questions to consider when concerning the influence of land surface forcing would be (1) whether land surface conditions reinforce the large-scale atmospheric circulation patterns? and (2) would they influence the persistence of wet or dry conditions on a regional scale? Further research into the physical forcing mechanisms of these dominant precipitation modes is necessary to assess the limits of warm season predictability in North America. The southwest and central United States are probably the two regions within the United States with the greatest

potential for improved warm season precipitation forecasts due to the influence of ENSO/PDV forcing.

As highlighted in Section 5, the results of this analysis will be used in a larger paleoclimate project to reconstruct NAM precipitation from ponderosa pine and Douglas-fir tree-rings around the southwest United States. An LAI extracted from the rings can serve as a proxy for NAM precipitation variability. On the basis of preliminary analysis done thus far with the rotated RPCs of 36 latewood adjusted tree-ring chronologies, the results are promising. The dominant spatial variability patterns of precipitation over the NAM region are reflected and comparable to that of the observed dominant modes. Notably, a comparable signature of ENSO/PDV in the SSTAs of the first LAI mode to dominant early summer mode is present. Thus, the latewood tree-ring data appear to be suitable as a proxy for precipitation and for extending that particular record of NAMS, and this will yield additional insight into its variability during southwest United States droughts over past centuries.

The dominant warm season precipitation modes revealed in this study will be used to answer two questions with respect to our analysis of dynamically downscaled global climate model data. First, are the warm season modes present in the RCM data reflected in the same way as in the observations during the period of historical record of the late 20th century? Second, do these modes change in the future to create more extreme climate by synergistically interacting with a long-term climate change signal?

Acknowledgements

Support for the 20th Century Reanalysis Project dataset is provided by the US Department of Energy, Office of Science Innovative and Novel Computational Impact on Theory and Experiment (DOE INCITE) program, and Office of Biological and Environmental Research (BER) and by the National Oceanic and Atmospheric Administration Climate Program Office. We thank Mr. Koichi Sakaguchi and Ms. Tracey Keller for their assistance in performing some of the analyses and construction of figures in this manuscript. Kapalan SST V2, Interpolated OLR, and NCEP Reanalysis data was provided by the NOAA/OAR/ESRL PSD, Boulder, Colorado, USA from their Website at http://www.esrl.noaa.gov/psd. This research was funded by the National Science Foundation under grants ATM-0813656 and the Climate Change Program Grant 0823090.

References

Adams DK, Comrie AC. 1997. The North American Monsoon. *Bulletin of the American Meteorological Society* **10**: 2197–2213.

Barlow M, Nigam S, Berbery EH. 1998. Evolution of the North American Monsoon system. *Journal of Climate* **11**: 2238–2257.

Barnett TP, Preisendorfer R. 1987. Origins and levels of monthly and seasonal forecast skill for United States surface air temperatures determined by canonical correlation analysis. *Monthly Weather Review* **115**: 1825–1850.

Biondi F, Gershunov A, Cayan DR. 2001. North Pacific decadal climate variability since 1661. *Journal of Climate* **14**: 5–10. DOI: 10.1175/1520-0442

Blackmon ML, Lee YH, Wallace JM, Hsu HH. 1984. Time variation of 500 mb height fluctuations with long, intermediate and short time scales as deduced from lag-correlation statistics (in synoptic atmospheric circulation). *Journal of Atmospheric Sciences* **41**: 981–991.

Carleton AM, Carpenter DA, Weser PJ. 1990. Mechanisms of interannual variability of the southwest United States summer rainfall maximum. *Journal of Climate* **3**: 999–1015. DOI: 10.1175/1520-0442

Castro CL, McKee TB, Pielke RA Sr. 2001. The relationship of the North American Monsoon to tropical and north Pacific sea surface temperatures as revealed by observational analysis. *Journal of Climate* **14**: 4449–4473. DOI: 10.1175/1520-0442

Castro CL, Pielke R Sr, Adegoke JO. 2007a. Investigation of the summer climate of the contiguous Unite States and Mexico using regional atmospheric modeling system (RAMS). Part I: model climatology (1950–2002). *Journal of Climate* **20**: 3844–3865. DOI: 10.1175/JCLI4211.1

Castro CL, Pielke RA Sr, Adegoke JO, Schubert SD, Pegion PJ. 2007b. Investigation of the summer climate of the contiguous United States and Mexico using Regional Atmospheric Modeling System (RAMS). Part II: model climate variability. *Journal of Climate* **20**: 3866–3887.

Castro CL, Beltrán-Prezekurat AB, Pielke RA Sr. 2009. Spatiotemporal variability of precipitation, modeled soil moisture, and vegetation greenness in North America within the recent observational record. *Journal of Hydrometeorology* **10**: 1355–1378. DOI: 10.1175/2009JHM1123.1

Compo GP, Whitaker JS, Sardeshmukh PD. 2006. Feasibility of a 100 year reanalysis using only surface pressure data. *Bulletin of the American Meteorological Society* **87**: 175–190.

Compo GP, Whitaker JS, Sardeshmukh PD, Matsui N, Allan RJ, Yin X, Gleason BE, Vose RS, Rutledge G, Bessemoulin P, Brönnimann S, Brunet M, Crouthamel RI, Grant AN, Ross PY, Trigo RM, Wang XL, Woodruff SD, Worley SJ. 2011. The twentieth century reanalysis project. *Quarterly Journal of the Royal Meteorological Society* **137**: 1–28. DOI: 10.1002/qj.776

Ding Q, Wang B. 2005. Circumglobal teleconnection in the Northern Hemisphere summer. *Journal of Climate* **18**: 3483–3505.

Ding Q, Wang B, Wallace JM, Branstator G. 2011. Tropical-extratropical teleconnections in boreal summer: observed interannual variability. *Journal of Climate* **24**: 1878–1896.

Englehart PJ, Douglas AV. 2006. Defining intraseasonal rainfall variability within the North American Monsoon. *Journal of Climate* **19**: 4243–4253.

Feng S, Hu Q, Oglesby RJ. 2011. Influence of Atlantic sea surface temerpatures on persistent drought in North America. *Climate Dynamics* **37**: 569–586.

Fritts HC. 1966. Growth-rings of trees: their correlation with climate. *Science* **154**: 973–979. DOI: 10.1126/science.154.3752.973

Gershunov A, Barnett TP. 1998. ENSO influence on intraseasonal extreme rainfall and temperature frequencies in the contiguous United States: observations and model results. *Journal of Climate* **11**: 1575–1586. DOI: 10.1175/1520-0442

Griffin D, Meko DM, Touchan R, Leavitt SW, Woodhouse CA. 2011. Latewood chronology development for summer moisture reconstruction in the U.S. Southwest. *Tree Ring Research* **67**: 87–101.

Gutzler DS. 2000. Covariability of spring snowpack and summer rainfall across the southwest United States. *Journal of Climate* **13**: 4018–4027.

Gutzler DS, Preston JW. 1997. Evidence for a relationship between spring snow cover in North America and summer rainfall in New Mexico. *Geophysical Research Letters* **24**: 2207–2210.

Gutzler DS, Kann DM, Thornbrugh C. 2002. Modulation of ENSO-based long-lead outlooks of southwestern U.S. winter precipitation by the Pacific Decadal Oscillation. *Weather and Forecasting* **17**: 1163–1172. DOI: 10.1175/1520-0434

Harrington JA Jr, Cerveny R, Balling R Jr. 1992. Impact of the Southern Oscillation on the North American southwest Monsoon. *Physical Geography* **13**: 318–330.

Heim HR Jr. 2002. A review of twentieth century drought indices used in the United States. *Bulletin of the American Meteorological Society* **83**: 1149–1165.

Higgins RW, Shi W. 2000. Intercomparison of the principal modes of interannual and intraseasonal variability of the North American Monsoon system. *Journal of Climate* **14**: 403–417.

Higgins RW, Yao Y, Wang XL. 1997. Influence of the North American Monsoon System on the U.S. summer precipitation regime. *Journal of Climate* **10**: 2600–2622. DOI: 10.1175/1520-0442

Higgins RW, Mo KC, Yao Y. 1998. Interannual variability of the U.S. summer precipitation regime with emphasis on the Southwestern Monsoon. *Journal of Climate* **11**: 2582–2606. DOI: 10.1175/1520-0442

Higgins RW, Chen Y, Douglas AV. 1999. Interannual variability of the North American warm season precipitation regime. *Journal of Climate* **12**: 653–680.

Higgins RW, Leetmaa A, Xue Y, Barnston A. 2000. Dominant factors influencing the seasonal predictability of U.S. precipitation and surface air temperature. *Journal of Climate* **13**: 3994–4017.

Horel JD, Wallace JM. 1981. Planetary-scale atmospheric phenomena associated with the Southern Oscillation. *Monthly Weather Review* **109**: 813–829.

Hoskins BJ, Simmons AJ, Andrews DG. 1977. Energy dispersion in a barotropic atmosphere. *Quarterly Journal of the Royal Meteorological Society* **103**: 553–567. DOI: 10.1002/qj.49710343802

Hu Q, Feng S. 2002. Interannual rainfall variations in the North American Monsoon region: 1900–98. *Journal of Climate* **15**: 1189–1202.

Hu Q, Feng S. 2008. Variation of North American summer monsoon regimes and the Atlantic multidecadal oscillation. *Journal of Climate* **21**: 2373–2383.

Jiang X, Lau NC. 2008. Intraseasonal teleconnection between North American and western North Pacific monsoons with 20-day time scale. *Journal of Climate* **21**: 2664–2679.

Kalnay E, Kanamitsu M, Kistler R, Collins W, Deaven D, Gandin L, Iredell M, Saha S, White G, Woollen J, Zhu Y, Leetmaa A, Reynolds R, Chelliah M, Ebisuzaki W, Higgins W, Janowiak J, Mo KC, Ropelewski C, Wang J, Jenne R, Joseph D. 1996. The NCEP/NCAR 40-year reanalysis project. *Bulletin of the American Meteorological Society* **77**: 437–471.

Kanamitsu M, Mo KC. 2003. Dynamical effect of land surface processes on summer precipitation over the southwestern United States. *Journal of Climate* **16**: 496–509 DOI: 10.1175/1520-0442(2003)016.

Kaplan A, Cane M, Kushnir Y, Clement A, Blumenthal M, Rajagopalan B. 1998. Analyses of global sea surface temperature 1856–1991. *Journal of Geophysical Research* **103**: 567–589.

Leathers DJ, Yarnal B, Palecki MA. 1991. The Pacific/North American teleconnection pattern and United States climate. Part I: Regional temperature and precipitation associations. *Journal of Climate* **4**: 517–528. DOI: 10.1175/1520-0442

Leavitt SW, Woodhouse CA, Castro CL, Wright WE, Meko DM, Touchan R, Griffin D, Ciancarelli B. 2011. The North American Monsoon in the U.S. Southwest: potential for investigation with tree-ring carbon isotopes. *The Journal of the International Union for Quaternary Research* **235**: 101–107 DOI: 10.1016/j.quaint.2010.05.006.

Liebmann B, Smith CA. 1996. Description of a complete (interpolated) outgoing longwave radiation dataset. *Bulletin of the American Meteorological Society* **77**: 1275–1277.

Liebmann B, Bladé I, Bond NA, Gochis D, Allured D, Bates GT. 2008. Characteristics of North American summertime rainfall with emphasis on the Monsoon. *Journal of Climate* **21**: 1277–1294. DOI: 10.1175/2007/JCLI1762.1

Livezey RE, Chen WY. 1983. Statistical field significance and its determination by Monte Carlo techniques (in meteorology). *Monthly Weather Review* **111**: 46–59.

Livezey RE, Mo KC. 1987. Tropical-extratropical teleconnections during the Northern Hemisphere winter. Part II: Relationships between monthly mean Northern Hemisphere circulation patterns and proxies for tropical convection. *Monthly Weather Review* **115**: 3115–3132.

Lo F, Clark MP. 2002. Relationships between spring snow mass and summer precipitation in the southwestern United States associated with the North American Monsoon system. *Journal of Climate* **15**: 1378–1385.

McCabe GJ, Dettinger MD. 1999. Decadal variations in the strength of ENSO teleconnections with precipitation in the western United States. *International Journal of Climatology* **19**: 1399–1410.

Mckee TB, Doesken NJ, Kleist J. 1993. The relationship of drought frequency and duration to time scales. In *Proceeding of the Ninth Conference on Applied Climatology*. American Meteorological Society: Boston; 179–184.

Meko DM, Baisan CH. 2001. Pilot study of latewood-width of conifers as an indicator of variability of summer rainfall in the North American Monsoon region. *International Journal of Climatology* **21**: 697–708. DOI: 10.1002/joc.646

Meko DM, Woodhouse CA, Baisan CH, Knight T, Lukas JJ, Hughes MK, Salzer MW. 2007. Medieval drought in the upper Colorado River basin. *Geophysical Research Letters* **34**: L10705. 10.1029/2007GL029988.

Mo KC, Paegle JN. 2000. Influence of sea surface temperature anomalies on the precipitation regimes over the southwest United States. *Journal of Climate* **13**: 3588–3598 DOI: 10.1175/1520-0442(2000)013.

Mo KC, Schemm JE. 2007. Droughts and persistent wet spells over the United States and Mexico. *Journal of Climate* **21**: 980–994. DOI: 10.1175/2007JCLI1616.1.

Mo KC, Paegle JN, Higgins RW. 1997. Atmospheric processes associated with summer floods and droughts in the central United States. *Journal of Climate* **10**: 3028–3046. 10.1175/1520-0442(1997)010.

Myoung B, Deng Y. 2009. Interannual variability of the cyclonic activity along the U.S. Pacific coast: Influences on the characteristics of winter precipitation in the western United States. *Journal of Climate* **22**: 5732–5747. DOI: 10.1175/2009CLI2889.1

Okabe IT. 1995. *The North American Monsoon*. PhD dissertation, University of British Columbia, 146 pp.

PRISM Climate Group. 2004. Parameter-elevation Regressions on Independent Slopes Model monthly precipitation grid. Available at http://www.prism.oregonstate.edu [2008].

Redmond KT, Koch RW. 1991. Surface climate and streamflow variability in the western United States and their relationship to large scale circulation indicies. *Water Resources Research* **27**: 2381–2399. DOI: 10.1029/91WR00690

Richman MB. 1986. Rotation of principal components. *International Journal of Climatology* **6**: 29–35.

Ropelewski CF, Halpert MS. 1986. North American precipitation and temperature associated with El Nino/Southern Oscillation (ENSO). *Monthly Weather Review* **114**: 2352–2362.

Ropelewski CF, Halpert MS. 1987. Global and regional scale precipitation patterns associated with the El Nino/Southern Oscillation. *Monthly Weather Review* **115**: 1606–1626.

Sardeshmukh PD, Hoskins BJ. 1988. The generation of global rotational flow by steady idealized tropical divergence. *Journal of Atmospheric Sciences* **45**: 1228–1251.

Schubert SD, Suarez MJ, Pegion PJ, Koster RD, Bacmeister JT. 2004. Causes of long-term drought in the U.S. Great Plains. *Journal of Climate* **17**: 485–503.

Stahle DW, Cleaveland MK, Grissiono-Mayer HD, Griffin DR, Fye FK, Therrell MD, Burnette D, Meko DM, Villanueva-Diaz J. 2009. Cool and warm-season precipitation reconstructions over western New Mexico. *Journal of Climate* **22**: 3720–3750.

Sutton RT, Hodson DLR. 2005. Atlantic Ocean forcing of North American and European summer climate. *Science Magazine* **309**: 115–118. DOI: 10.1126/science.1109496

Tardy AO. 2010. The 2009–2010 extreme precipitation deficit and record heat in south Texas: Worst drought on record followed by a cold and wet winter. National Weather Association Annual Meeting: Tucson; October 3–9.

Therrell MD, Stahle DW, Cleaveland MK, Villanueva-Diaz J. 2002. Warm season tree growth and precipitation over Mexico. *Journal of Geophysical Research* **107**: 4205–4212. DOI: 10.1029/2001JD000851

Trenberth KE. 1990. Recent observed interdecadal climate changes in the Northern Hemisphere. *Bulletin of the American Meteorological Society* **71**: 988–993.

Wallace JM, Gutzler DS. 1981. Teleconnections in geopotential height field during the Northern Hemisphere winter. *Monthly Weather Review* **109**: 784–812.

Weiss JL, Castro CL, Overpeck JT. 2009. Distinguishing pronounced droughts in the southwestern United States: seasonality and effects of warmer temperatures. *Journal of Climate* **22**: 5918–5932. DOI: 10.1175/2009JCLI2905.1

Wilks DS. 2006. *Statistical Methods in the Atmospheric Sciences*. Elsevier: Burlington.

Woodhouse CA, Gray ST, Meko DM. 2006. Updated streamflow reconstructions for the upper Colorado River basin. *Water Resources Research* **42**: W05415. DOI: 10.1029/2005WR004455.

Zhu C, Lettenmaier DP, Cavazos T. 2005. Role of antecedent land surface conditions on North American Monsoon rainfall variability. *Journal of Climate* **18**: 3104–3121.

